frontiers in Earth Science

ORIGINAL RESEARCH
published: 13 May 2020
doi: 10.3389/feart.2020.00053

Comparing Aggradation, Superelevation, and Avulsion Frequency of Submarine and Fluvial Channels

Zane R. Jobe[1], Nick C. Howes[2], Kyle M. Straub[3], Dingxin Cai[1], Hang Deng[1], Fabien J. Laugier[4], Luke A. Pettinga[1] and Lauren E. Shumaker[1]*

[1] Colorado School of Mines, Golden, CO, United States, [2] Mathworks, Natick, MA, United States, [3] Tulane University, New Orleans, LA, United States, [4] Chevron Energy Technology Company, Houston, TX, United States

Constraining the avulsion dynamics of rivers and submarine channels is essential for predicting the distribution of sediment, organic matter, and pollutants in alluvial, deltaic, and submarine settings. We create a geometric channel-belt framework relating channel, levee, and floodplain stratigraphy that allows comparative analysis of avulsion dynamics for rivers and submarine channels. We utilize 52 channel-overbank cross-sections within this framework to provide avulsion criteria for submarine channels, and how they differ from rivers. Superelevation and a new channel-floodplain coupling metric are two key parameters that control channel-belt thickness in both rivers and submarine channels. While rivers only superelevate 1 channel depth above the floodplain prior to avulsion, submarine channels are more stable during aggradation, with superelevation values commonly > 3 channel depths. Additionally, channel-floodplain coupling in rivers is often weak, with floodplain aggradation negligible compared to channel aggradation, making rivers avulsion-prone. However, floodplain aggradation is more significant for submarine channels, resulting in stronger channel-floodplain coupling and thus a decreased potential for avulsion. The combination of enhanced superelevation and strong channel-floodplain coupling results in submarine channel-belts that can be as thick as ∼10 channel depths, while fluvial channel belts are limited to 2 channel depths. Submarine channels are more stable because turbidity currents have ∼50x lower density contrast between flow and ambient fluid as compared to rivers. This density contrast creates far less potential energy for avulsion, despite the much greater relief of submarine levees compared to fluvial levees. The modern Amazon submarine channel showcases this stability, with a channel belt that is ∼5 channel-depths thick for more than 400 streamwise km, which is more than twice the superelevation that a river is capable of. We interpret that enhanced floodplain aggradation and levee aggradation (and thus superelevation) in submarine channel belts are promoted by unique submarine flow characteristics, including turbidity current overspill, flow-stripping, and hemipelagic processes. We emphasize that rivers and submarine channels display very different avulsion dynamics and frequencies, profoundly affecting the stratigraphic architecture of channel-belt and downstream distributary deposits.

Keywords: turbidite, scaling relationships, submarine fan, morphodynamics, river

OPEN ACCESS

Edited by:
Amanda Owen, University of Glasgow, United Kingdom

Reviewed by:
David Mark Hodgson, University of Leeds, United Kingdom
Maria Ansine Jensen, The University Centre in Svalbard, Norway

****Correspondence:***
Zane R. Jobe
zanejobe@gmail.com

Specialty section:
This article was submitted to Sedimentology, Stratigraphy and Diagenesis, a section of the journal Frontiers in Earth Science

Received: *30 August 2019*
Accepted: *13 February 2020*
Published: *13 May 2020*

Citation:
Jobe ZR, Howes NC, Straub KM, Cai D, Deng H, Laugier FJ, Pettinga LA and Shumaker LE (2020) Comparing Aggradation, Superelevation, and Avulsion Frequency of Submarine and Fluvial Channels. Front. Earth Sci. 8:53. doi: 10.3389/feart.2020.00053

INTRODUCTION

Rivers and submarine channels carry and distribute sediment, organic matter, pollutants around the world (Hodgson et al., 2018; Kane and Clare, 2019), and it is of paramount importance to understand the dynamics controlling sediment distribution in these channelized depositional systems. Rivers and submarine channels have similar planform morphologies (Flood and Damuth, 1987; Pirmez and Imran, 2003; Kolla et al., 2007) but with markedly different preserved stratigraphic architecture due primarily to differences in channel aggradation during channel-belt evolution (Imran et al., 1998, 1999; Peakall et al., 2000; Jobe et al., 2016). A channel belt is typically defined as the genetic deposits of one avulsion cycle (Leeder, 1978; Bridge and Leeder, 1979). In this study, the channel belt encompasses all channel-related sediment in one avulsion cycle (thalweg, bar, splay, internal and external levee, and floodplain deposits; **Figures 1**, **2**). Aggradation of the channel above the floodplain results in storage of potential energy in the flow to cause an avulsion (Imran et al., 1998; Mohrig et al., 2000). For rivers, this potential energy is high because of the large excess density between the flow (water) and the ambient fluid (air; Imran et al., 1998), resulting in rivers that can only reach 1 channel depth above the floodplain before avulsion (Mohrig et al., 2000). In submarine channels sculpted by turbidity currents, however, the potential energy is much lower due to the relatively small excess density between a turbidity current and the ambient seawater, leading to taller external levees and less frequent avulsion (Imran et al., 1998). However, the amount of pre-avulsion aggradation possible in submarine channel-belts has never been quantified.

In both rivers and submarine channels, avulsion is an important process for the construction of fluvial (Heller and Paola, 1996; Ganti et al., 2016) and submarine stratigraphic architecture (Flood et al., 1991; Torres et al., 1997; Schwenk et al., 2003). Avulsion is defined as the process by which flow is diverted out of an established channel belt into a new flow pathway on the adjacent floodplain (Mohrig et al., 2000; Slingerland and Smith, 2004). For avulsion to occur, the channel belt must aggrade above the adjacent floodplain to create a favorable potential energy gradient (i.e., the 'setup'; Bridge and Leeder, 1979; Bryant et al., 1995; Heller and Paola, 1996; Mohrig et al., 2000) and there must be a trigger/initiation event (Jones and Schumm, 1999). Sometimes, these criteria are met but the channel does not avulse, generating crevasse-splay deposits that further help to aggrade the channel-belt (Burns et al., 2017; Nienhuis et al., 2018; van Toorenenburg et al., 2018).

River avulsions are well-studied, and numerous avulsions have been observed during historic times (e.g., Smith et al., 1989). Avulsion setup criteria for rivers are well-constrained (Mohrig et al., 2000; Ganti et al., 2016) and documented triggers are commonly levee breaches during floods (e.g., Slingerland and Smith, 1998, 2004). Although a specific event (e.g., a levee failure) can trigger avulsion, normal overspill from a bankfull flow may be enough to generate channel avulsions (Edmonds et al., 2009), particularly when avulsion criteria have been reached.

In submarine channel settings, no historical avulsions have been observed or documented, and both the setup and triggering mechanisms are poorly constrained. Most work has focused not on the setup, but instead on interpreting triggers, which include flow-overspill and flow-stripping (Piper and Normark, 1983; Fildani et al., 2006), channel-floor aggradation (Kolla, 2007; Armitage et al., 2012), levee failure by mass-wasting (Flood et al., 1991; Brunt et al., 2013), mass-transport deposition/erosion (Ortiz-Karpf et al., 2015), and climate cyclicity (Picot et al., 2019). Avulsion triggers are difficult to predict due to their dependence on local factors and their opportunistic nature (Slingerland and Smith, 2004); however, the setup can easily be measured and constrained using the abundant seafloor, seismic reflection, and core data that documents Quaternary submarine channel avulsions (e.g., Pirmez and Flood, 1995; Manson, 2009 for the Amazon, Torres et al., 1997 for the Rhone). In this study, we document aggradation metrics and develop avulsion setup criteria for leveed, aggradational submarine channels. We also develop a theory for coupling between channels and their associated floodplains and explore differences between fluvial and submarine channel-floodplain coupling and the implications for channel-belt stability and avulsion frequency.

GOVERNING EQUATIONS

Superelevation

The relative superelevation (S_E) is defined as the relief between the levee crest (L_R) and the adjacent floodplain, normalized by the channel depth (H; Eq. 1) (Bryant et al., 1995; Mohrig et al., 2000). Superelevation (S_E) of the channel should not be confused with superelevation of the water/flow surface at the apex of a meander bend due to centrifugal acceleration (Dietrich and Whiting, 1989 for riverine flow; Hay, 1987 for turbidity currents).

Equation 1, avulsion criterion for rivers using relative superelevation:

$$S_E = \frac{L_R}{H}$$

A superelevation $S_E = 1$ indicates that the channel thalweg is at the same elevation as the floodplain (i.e., the elevation of the levee crest is 1 channel depth above the floodplain); data from modern and ancient fluvial systems (Mohrig et al., 2000; Jerolmack, 2009) suggest this value is a practical maximum for rivers. In other words, the avulsion setup is complete when the channel is superelevated one channel depth above the surrounding floodplain and only a trigger event is required to cause an avulsion. The rationale for this maximum value of S_E is that by the time the channel thalweg reaches the elevation of the adjacent floodplain ($S_E \sim 1$), there is sufficient potential energy for avulsion to take place (Imran et al., 1998; Mohrig et al., 2000).

Tall and thick external levees and a channel perched high above the submarine floodplain have long been recognized in submarine settings (Buffington, 1952; Damuth and Flood, 1983; Hübscher et al., 1997) and explained by the flow properties of turbidity currents (Imran et al., 1998, 1999). We use the term floodplain to describe the far-field overbank areas of submarine

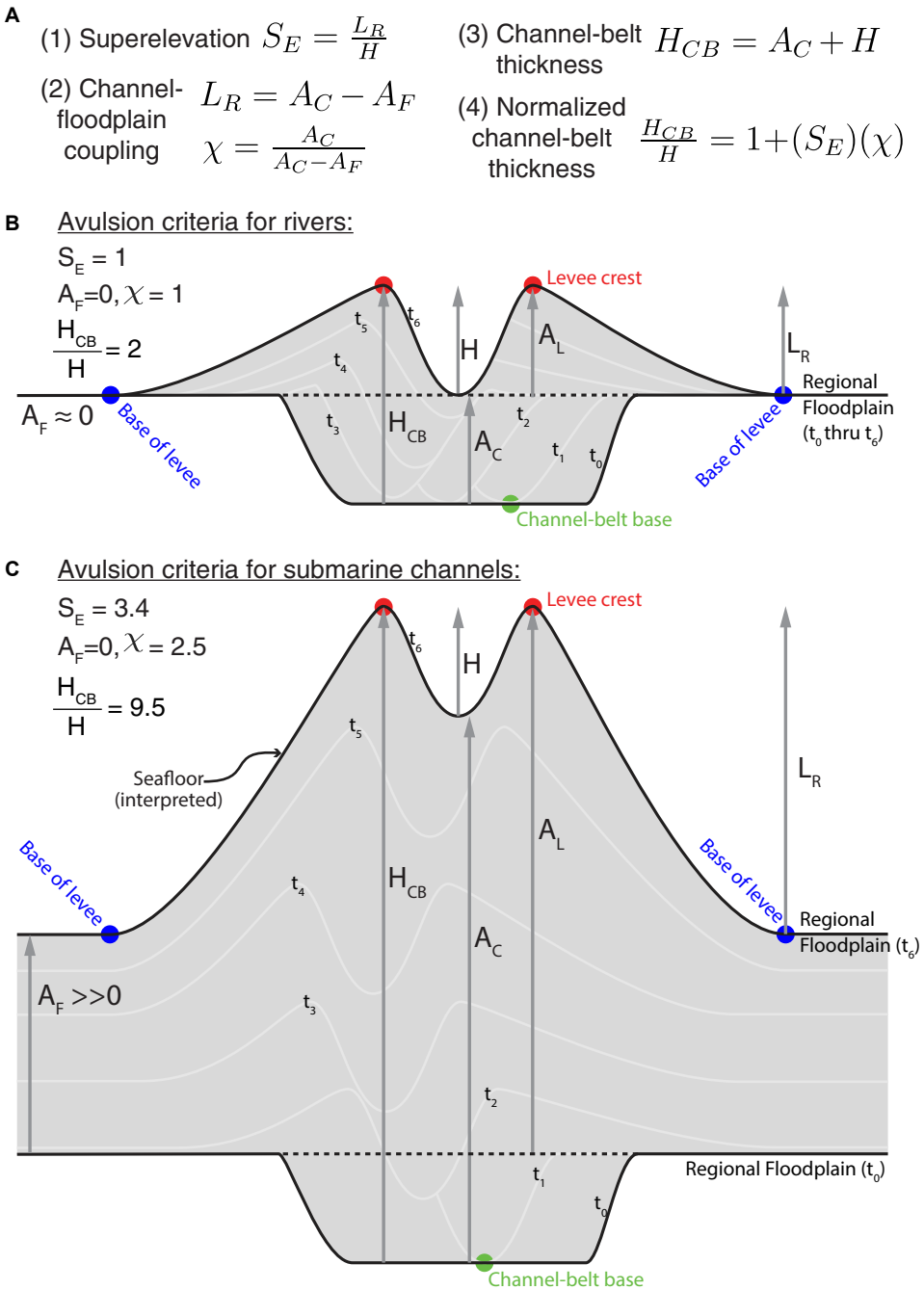

FIGURE 1 | Fluvial and submarine channel-belt metrics for measuring aggradation and determining avulsion criteria. **(A)** Governing equations (see text for explanation of terms). **(B)** Fluvial channel-belt diagram and avulsion criteria. **(C)** Submarine channel diagram and avulsion criteria. Submarine channels can be up to 10 times thicker than rivers at avulsion due to enhanced superelevation and channel-floodplain coupling.

channel-belts for simplicity and consistency when comparing to rivers. Levee relief above the floodplain has also been documented for many submarine channels (e.g., Pirmez and Imran, 2003; Babonneau et al., 2010; compilation of Nakajima and Kneller, 2012) and shown to be larger than that of rivers; however, superelevation and how it evolves through channel-belt evolution has never before been compiled for submarine settings, nor has a maximum S_E value been proposed as an avulsion criteria for submarine channels.

Channel-Floodplain Coupling

Superelevation theory (Eq. 1; Mohrig et al., 2000) is useful for characterizing modern geomorphological parameters for rivers. However, we are interested in the preserved record of

channel-belt evolution and the potential coupling between the channel and its floodplain. Hence, we use parameters that can be measured from the preserved stratigraphic record to define a geometric equation that governs the amount of coupling between the channel and its floodplain in both fluvial and submarine settings (**Figure 1**):

Equation 2, Channel-floodplain coupling (fluvial and submarine):

$$L_R = A_C - A_F, \text{ where } A_C = A_L$$

This geometric coupling equation relates the aggradation of the levee and floodplain to the channel aggradation, where L_R is levee relief, A_C is channel aggradation, A_F is floodplain aggradation, and A_L is levee aggradation (**Figure 1**). The necessary conditions to form this geometric relationship are: (1) channel depth H must be constant during channel evolution for A_C and A_L to be equal, (2) $L_R = 0$ at channel initiation (**Figure 1**), and (3) channels are net aggradational. We acknowledge that H is spatially and temporally variable in both fluvial (Nittrouer et al., 2011) and submarine (Shumaker et al., 2018) channels, but this assumption is made for simplicity. We also acknowledge that many fluvial and submarine channels evolve through an incisional phase (e.g., Strong and Paola, 2008; Sylvester et al., 2011; Jobe et al., 2016), but this study is focused on aggradational channels that have well-defined external levees (*sensu* Kane and Hodgson, 2011) and lack a significant incisional phase (e.g., the Amazon submarine channel, Pirmez and Flood, 1995).

Channel-Floodplain Coupling in Rivers

In rivers, A_F is here considered negligible because channel-belt deposition (A_C, A_L) will be much more rapid than far-field, distal floodplain aggradation (**Figure 1**; Wolman and Leopold, 1957; Leeder, 1978; Bridge and Leeder, 1979; Brizga and Finlayson, 1990; Jerolmack and Paola, 2007; Hajek and Edmonds, 2014). We acknowledge that $A_F = 0$ is an assumption that may not be valid for all rivers, but available data from modern rivers validate this assumption: numerous aggradation rate measurements from modern floodplains demonstrate that A_C is 10–55 times greater than A_F (Bridge and Leeder, 1979; Pizzuto, 1987; Törnqvist and Bridge, 2002; Jerolmack and Paola, 2007; Aalto et al., 2008). This indicates very weak coupling between the aggradation of the channel and its floodplain for rivers.

If $A_F = 0$, Eq. 2 can be re-written as:

Equation 3, Fluvial channel-floodplain coupling,

$$\text{where } A_F = 0\text{: } A_C = L_R$$

We assume a simplified (i.e., flat) floodplain, while acknowledging that floodplain topography/dynamics can be complex (Lewin and Ashworth, 2014; Nienhuis et al., 2018; Johnston et al., 2019), affecting crevasse/avulsion location (Jerolmack and Paola, 2007) and crevasse/avulsion style (Hajek and Edmonds, 2014; Burns et al., 2017). The theory in Eq. 3 is also restricted to normal-flow fluvial reaches upstream of the backwater limit (the location where the mean elevation of the riverbed drops below sea-level or lake-level; Nittrouer et al., 2011). In the backwater zone, the sediment-transport regime is modified by spatial and temporal flow non-uniformity (Nittrouer et al., 2011), which affects channel-floor aggradation and scouring (Nittrouer et al., 2011, 2012), reduces levee growth and relief (Ganti et al., 2016), and changes channel belt dynamics and dimensions (Fernandes et al., 2016; Martin et al., 2018). Due to these complex hydro- and morpho-dynamics, this study will not further discuss coastal/backwater river systems, instead focusing on the differences between submarine channels and alluvial river reaches upstream of the backwater limit.

Channel-Floodplain Coupling in Submarine Channels

Floodplain aggradation A_F in submarine channel settings must be considered a non-zero value, as it often attains a thickness that is comparable to other channel-belt thickness metrics (e.g., A_L, A_C, H; **Figure 1**). We use the term 'floodplain' to describe the far-field overbank areas of submarine channel-belts for simplicity and consistency when comparing to rivers; other terms like 'overbank wedge' (Normark et al., 1993), 'distal external levee' (Kane and Hodgson, 2011; Morris et al., 2014, 2016), 'far-field overbank,' 'open slope,' and 'basin plain' are commonly used for this submarine geomorphic area (depending on the documented/inferred slope position of the channel-belt) and are synonymous to floodplain in this study.

Enhanced floodplain aggradation in submarine channel settings is influenced by turbidity current overspill and flow stripping (Piper and Normark, 1983; Hiscott et al., 1997; Straub et al., 2008), overbanking dilute, sheet-like turbidity currents (Stow and Piper, 1984; Straub and Mohrig, 2008; Jobe et al., 2011; Shumaker et al., 2017), and hemipelagic deposition (Stow et al., 2001). Unfortunately, datasets with paired channel and floodplain aggradation rate data do not exist, but several examples contain paired channel and levee-crest aggradation rates, demonstrating the importance of floodplain deposition in submarine channel belts. In the Bengal submarine channel, floodplain aggradation rates are ∼50 cm/ky (core 120KL) when levee-crest aggradation rates are ∼100 cm/ky (core 118KL, Weber et al., 1997). In the Amazon submarine channel, levee-crest aggradation rates are 360–517 cm/ky (sites 936, 946) while floodplain aggradation rates are 50–125 cm/ky (sites 930, 932, 935) (Mikkelsen et al., 1997). These two examples indicate that A_C is only 2–10 times greater than A_F, and thus A_F cannot be neglected in submarine settings (**Figure 1**), and Eq. 2 is modified accordingly:

Equation 4, Submarine channel-floodplain coupling,

$$\text{where } A_F > 0\text{: } \frac{A_C}{L_R} > 1$$

This suggests that for a given channel dimension, submarine channel-belts will be systematically thicker than a fluvial channel-belt due to a positive A_F (**Figure 1**) and greater levee relief (Buffington, 1952; Damuth and Flood, 1983). While Dorrell et al. (2015) demonstrate that aggrading submarine channels eventually become unstable and avulse due to geometric constraints, we suggest that submarine channel-floodplain

coupling is stronger than that in rivers, and as a result submarine channels are more stable than rivers under aggradational conditions (i.e., with $S_E > 1$, see **Figure 1**). A compilation of data from rivers and submarine channel belts (Jobe et al., 2016) supports this hypothesis.

Channel-Belt Thickness: Combining Superelevation and Coupling Parameters

Figure 1 shows the geometric relationships between the various measurable channel-belt parameters, and these can be arranged to define the thickness of the channel belt (H_{CB}) by relating the channel depth H and the aggradation of the channel A_C:

Equation 5A, Channel-belt thickness for fluvial and submarine channels

$$H_{CB} = H + A_C$$

Equation 5B, Normalized channel-belt thickness

$$\frac{H_{CB}}{H} = 1 + \frac{A_C}{H}$$

Because H tends to be quite variable between (and sometimes within) systems (Shumaker et al., 2018), normalized channel-belt thickness (Eq. 5B also see Jobe et al., 2016) is preferred when comparing systems, and we will subsequently use this form. By expanding the A_C/H term in Eq. 5B to include L_R, we obtain a more general form that defines channel-belt thickness using a dimensionless superelevation term and a dimensionless coupling term:

Equation 6. Channel belt thickness

$$\frac{H_{CB}}{H} = 1 + \left(\frac{L_R}{H}\right)\left(\frac{A_C}{L_R}\right)$$

We can further modify the A_C/L_R term in Eq. 6 by utilizing the relationship in Eq. 2 to derive;

Equation 7. Channel-floodplain coupling parameter

$$\frac{A_C}{L_R} = \frac{A_C}{A_C - A_F} = \chi$$

The parameter χ describes channel-floodplain coupling without using L_R or H, which define the superelevation parameter S_E (Eq. 1). Substituting χ and S_E into Eq. 6, we can rewrite the final form of the channel-belt thickness equation as:

Equation 8, Channel-belt thickness with superelevation and channel-floodplain coupling terms:

$$\frac{H_{CB}}{H} = 1 + (S_E)(\chi)$$

Using Eq. 8 and our understanding of channel-belt evolution and avulsion, we can estimate H_{CB} when avulsion occurs for both fluvial and submarine settings.

Fluvial Conditions for Avulsion

Rivers have well-documented avulsions and the avulsion setup is well-constrained (Bridge and Leeder, 1979; Smith et al., 1989). In particular, Mohrig et al. (2000) established a superelevation criteria for river crevasse development and avulsion, with $S_E \sim 1$ at avulsion. Under the condition where H remains constant through channel-belt construction, fluvial channels become unstable and are prone to avulse when $H = L_R = A_C = A_L$ (**Figure 1**; Eq. 1). Assuming $A_F = 0$ for rivers (see section "Discussion" above, Eq. 3), the avulsion criteria for rivers can therefore be summarized as:

$$A_F \approx 0, \quad S_E = 1, \quad \chi = 1$$

Solving Eq. 8 using these values, the normalized channel-belt thickness for a river at avulsion is 2 (i.e., $H_{CB}/H = 2$; also see **Figure 1**). This is consistent with superelevation theory (Mohrig et al., 2000) as well as channel-floodplain coupling discussed above.

Submarine Conditions for Avulsion

For submarine channel belts, very little data has been collected on measurable parameters as compared to rivers. However, levee relief values are extremely large compared to channel depth in active channels (Damuth and Flood, 1983; Hübscher et al., 1997), suggesting that submarine channels are more stable at higher S_E values than rivers (cf. Dorrell et al., 2015). Floodplain aggradation is significant (Mikkelsen et al., 1997; Weber et al., 1997) and cannot be ignored. Thus, we can summarize the avulsion criteria for submarine channels as:

$$A_F > 0, \quad S_E > 1, \quad \chi > 1$$

Hence, if we solve Eq. 8 using these values, $H_{CB}/H > 2$ and potentially $> > 2$ (**Figure 1**). It is the aim of this paper to determine these values more precisely for submarine channel belts and quantify exactly how much more aggradational submarine channels are than rivers prior to avulsion.

DATA COLLECTION METHODOLOGY

We restricted our study to submarine channel-belts that have external levees and a relatively simple evolutionary history, excluding those channels that are purely incisional (i.e., canyons, Normark et al., 1993), had a complex incisional phase prior to aggrading (e.g., Kolla et al., 2012), or complex internal-levee architecture (Kane and Hodgson, 2011). Since we are interested in the aggradation of the channel-belt through time, bathymetric profiles do not provide enough information; rather, seismic-reflection profiles are needed to constrain the base of the channel belt. The five submarine channel-belts that met these criteria and had high-quality seismic-reflection data are the Amazon, Zaire, Danube, Rhone, Magdalena, and Mississippi (**Table 1**). Submarine channel-belt cross-sections in our compilation were

TABLE 1 | Parameters for 52 cross-sections of submarine channel belts used in this study.

Name	System	Source	Cross-section orientation (degrees from being perpendicular to flow direction)	Channel width (B, m)	Channel depth (H, m)	Channel belt thicknees (Hcb, m)	Levee relief (Lr, m)	Floodplain aggradation (Af, m)	Channel aggradation (Ac, m)	Superelevation (Se)	Coupling parameter (X)	Vertical units of cross-section	Depth conversion parameter	Unique ID
Amazon_F23-13_Flood1991	Amazon	Flood et al., 1991	17	2353	33	290	146	92	257	4.42	1.56	Time (sec)	1500 m/s	7
Amazon_F23-2A_Flood1991	Amazon	Flood et al., 1991	12	2685	147	498	172	331	350	1.17	18.42	Time (sec)	1500 m/s	52
Amazon_F4_Lopez2001	Amazon (not modern)	Lopez, 2001	40	758	42	256	55	152	213	1.31	3.49	Depth	n/a	29
Amazon_F4-11_Manson2009a	Amazon	Manson, 2009	9	409	59	163	91	41	103	1.54	1.66	Time (msec)	1500 m/s	8
Amazon_F4-11_Manson2009b	Amazon	Manson, 2009	14	814	35	245	125	71	210	3.57	1.51	Time (msec)	1500 m/s	9
Amazon_F4-11_Manson2009c	Amazon	Manson, 2009	16	537	43	235	108	71	192	2.51	1.59	Time (msec)	1500 m/s	10
Amazon_F4-11_Manson2009d	Amazon	Manson, 2009	56	384	11	243	71	53	231	6.45	1.30	Time (msec)	1500 m/s	11
Amazon_F4-11_Manson2009e	Amazon	Manson, 2009	0	1026	52	300	84	74	248	1.62	1.43	Time (msec)	1500 m/s	12
Amazon_F4-11_Manson2009f	Amazon	Manson, 2009	17	950	43	330	149	58	286	3.47	1.25	Time (msec)	1500 m/s	13
Amazon_F4-15A_Manson2009a	Amazon	Manson, 2009	34	555	40	40	6	22	0	0.15	0.00	Time (msec)	1500 m/s	14
Amazon_F4-15A_Manson2009b	Amazon	Manson, 2009	22	540	17	98	44	26	81	2.59	1.47	Time (msec)	1500 m/s	15
Amazon_F4-15A_Manson2009c	Amazon	Manson, 2009	16	449	29	93	41	38	63	1.41	2.52	Time (msec)	1500 m/s	16
Amazon_F4-15A_Manson2009d	Amazon	Manson, 2009	45	424	36	127	57	51	91	1.58	2.28	Time (msec)	1500 m/s	17

(Continued)

TABLE 1 | Continued

Name	System	Source	Cross-section orientation (degrees from being perpendicular to flow direction)	Channel width (B, m)	Channel depth (H, m)	Channel belt thicknees (Hcb, m)	Levee relief (Lr, m)	Floodplain aggradation (Af, m)	Channel aggradation (Ac, m)	Superelevation (Se)	Coupling parameter (X)	Vertical units of cross-section	Depth conversion parameter	Unique ID
Amazon_F4-15A_Manson2009e	Amazon	Manson, 2009	15	457	18	152	61	66	134	3.39	1.97	Time (msec)	1500 m/s	18
Amazon_F4-15A_Manson2009f	Amazon	Manson, 2009	18	520	44	121	52	53	77	1.18	3.21	Time (msec)	1500 m/s	19
Amazon_F4-15A_Manson2009h	Amazon	Manson, 2009	9	337	35	164	80	61	129	2.29	1.90	Time (msec)	1500 m/s	20
Amazon_F4-15A_Manson2009i	Amazon (1E)	Manson, 2009	3	618	10	34	12	12	23	1.20	2.09	Time (msec)	1500 m/s	21
Amazon_F4-15A_Manson2009j	Amazon (1E)	Manson, 2009	46	372	14	62	15	28	48	1.07	2.40	Time (msec)	1500 m/s	22
Amazon_F4-15A_Manson2009k	Amazon (1E)	Manson, 2009	16	387	12	59	25	25	46	2.08	2.19	Time (msec)	1500 m/s	23
Amazon_F4-15A_Manson2009l	Amazon (Brown)	Manson, 2009	33	489	15	101	41	34	85	2.73	1.67	Time (msec)	1500 m/s	50
Amazon_F4-15A_Manson2009m	Amazon (Brown)	Manson, 2009	6	302	10	84	36	32	73	3.60	1.78	Time (msec)	1500 m/s	51
Amazon_F4-15B_Manson2009a	Amazon	Manson, 2009	14	527	32	237	96	91	204	3.00	1.81	Time (msec)	1500 m/s	24
Amazon_F4-15B_Manson2009b	Amazon	Manson, 2009	16	548	27	226	86	98	199	3.19	1.97	Time (msec)	1500 m/s	25
Amazon_F4-15B_Manson2009c	Amazon	Manson, 2009	56	370	13	242	66	86	228	5.08	1.61	Time (msec)	1500 m/s	26
Amazon_F4-15B_Manson2009d	Amazon	Manson, 2009	0	1026	51	295	71	99	244	1.39	1.68	Time (msec)	1500 m/s	27

(Continued)

TABLE 1 | Continued

Name	System	Source	Cross-section orientation (degrees from being perpendicular to flow direction)	Channel width (B, m)	Channel depth (H, m)	Channel belt thicknees (Hcb, m)	Levee relief (Lr, m)	Floodplain aggradation (Af, m)	Channel aggradation (Ac, m)	Superelevation (Se)	Coupling parameter (X)	Vertical units of cross-section	Depth conversion parameter	Unique ID
Amazon_F4-15B_Manson2009e	Amazon	Manson, 2009	17	1086	45	326	93	60	280	2.07	1.27	Time (msec)	1500 m/s	28
Amazon_F16_Pirmez1995	Amazon	Pirmez and Flood, 1995	29	1647	123	232	120	77	109	0.98	3.41	Time (sec)	1500 m/s	1
Amazon_F17_Pirmez1995	Amazon	Pirmez and Flood, 1995	35	1533	69	270	67	106	200	0.97	2.13	Time (sec)	1500 m/s	2
Amazon_F18_Pirmez1995	Amazon	Pirmez and Flood, 1995	53	1879	37	345	110	186	307	2.97	2.54	Time (sec)	1500 m/s	3
Amazon_F19_Pirmez1995	Amazon	Pirmez and Flood, 1995	27	854	26	238	66	88	211	2.54	1.72	Time (sec)	1500 m/s	4
Amazon_F20_Pirmez1995	Amazon	Pirmez and Flood, 1995	2	896	15	188	96	48	172	6.40	1.39	Time (sec)	1500 m/s	5
Amazon_F21_Pirmez1995	Amazon	Pirmez and Flood, 1995	1	1174	41	150	42	48	109	1.02	1.79	Time (sec)	1500 m/s	6
Amazon_Fig11_Pirmez1997	Amazon	Pirmez et al., 1997	3	685	14	159	90	52	144	6.43	1.57	Time (sec)	1500 m/s	32
Danube_F1_Popescu2001a	Danube	Popescu et al., 2001	33	2242	101	509	347	177	408	3.44	1.77	Depth	n/a	33
Danube_F1_Popescu2001b	Danube	Popescu et al., 2001	20	571	20	88	38	43	68	1.90	2.72	Depth	n/a	34
Danube_F2_Popescu2001	Danube	Popescu et al., 2001	16	1395	140	459	262	105	318	1.87	1.49	Depth	n/a	35
Magdalena_F3_Leslie2011	Magdalena, Colombia	Leslie et al., 2011	12	1393	100	364	137	90	264	1.37	1.52	Time (sec)	1500 m/s	36
Mississippi_F9c_Stelting1986	Mississippi	Stelting et al., 1986	28	1485	19	244	46	175	225	2.42	4.50	Time (sec)	1500 m/s	37
Rhone_F5_Bonnel2005_aban	Rhone	Bonnel et al., 2005	2	1165	27	288	92	179	260	3.41	3.21	Depth	n/a	39
Rhone_F5_Bonnel2005_neo	Rhone	Bonnel et al., 2005	1	1360	11	68	20	31	56	1.82	2.24	Depth	n/a	38

(Continued)

TABLE 1 | Continued

Name	System	Source	Cross-section orientation (degrees from being perpendicular to flow direction)	Channel width (B, m)	Channel depth (H, m)	Channel belt thicknees (Hcb, m)	Levee relief (Lr, m)	Floodplain aggradation (Af, m)	Channel aggradation (Ac, m)	Superelevation (Se)	Coupling parameter (X)	Vertical units of cross-section	Depth conversion parameter	Unique ID
Rhone_F12_ Torres1997	Rhone	Torres et al., 1997	6	883	19	380	147	212	361	7.74	2.42	Time (msec)	1500 m/s	40
Zaire_F4A_ Droz2003	Zaire	Droz et al., 2003	18	1573	54	185	41	65	131	0.76	1.98	Time (sec)	1500 m/s	42
Zaire_F4B_ Droz2003a	Zaire	Droz et al., 2003	6	785	39	174	41	51	134	1.05	1.61	Time (sec)	1500 m/s	43
Zaire_F4B_ Droz2003b	Zaire	Droz et al., 2003	6	722	23	122	65	25	98	2.83	1.34	Time (sec)	1500 m/s	44
Zaire_F5-14_ Manson2009a	Zaire	Manson, 2009	27	1663	47	86	28	31	38	0.60	5.43	Time (msec)	1500 m/s	30
Zaire_F5-14_ Manson2009b	Zaire	Manson, 2009	7	1906	104	109	56	41	5	0.54	−0.14	Time (msec)	1500 m/s	31
Zaire_F4_ Marsset2009	Zaire	Marsset et al., 2009	15	2893	233	233	8	45	0	0.03	0.00	Time (sec)	1500 m/s	41
Zaire_Fig11_ Picot2016	Zaire	Picot et al., 2016	26	548	14	89	18	16	74	1.29	1.28	Time (sec)	1500 m/s	45
Zaire_Fig13_ Picot2016a	Zaire	Picot et al., 2016	10	1099	162	162	62	22	0	0.38	0.00	Time (sec)	1500 m/s	46
Zaire_Fig13_ Picot2016b	Zaire	Picot et al., 2016	4	615	16	22	6	16	5	0.38	−0.45	Time (sec)	1500 m/s	47
Zaire_Fig13_ Picot2016c	Zaire	Picot et al., 2016	20	526	12	32	6	17	20	0.50	6.67	Time (sec)	1500 m/s	48
Zaire_Fig13_ Picot2016d	Zaire	Picot et al., 2016	21	1129	31	48	2	8	17	0.06	1.89	Time (sec)	1500 m/s	49

selected to (1) include extant channels on the seafloor (i.e., not necessarily active but not buried or compacted), (2) not be affected by large faults or other allogenic factors, and (3) be approximately perpendicular to the channel (see **Table 1**) so that measurements of channel and channel-belt dimensions are accurate (i.e., no artificially wide channels due to oblique cross-sections). In planform view, the 52 cross-sections are, on average, within 19° of perpendicular to the local downstream direction of the channel (**Table 1**). If a cross-section displayed two-way travel time as the vertical unit, we converted to meters using a seawater velocity of 1500 m/s (i.e., 100 ms TWT = 75 m). While the shallow subsurface often has velocities 1400–2000 m/s (e.g., Flood et al., 1997), and we acknowledge that using 1500 m/s may slightly underestimate subsurface thickness, this value most accurately represents the seafloor surface, which is important for our calculations of L_R and H.

Coupling between the channel and the floodplain for any channelized setting can be described by measuring four channel-belt parameters: the channel depth H, levee relief above the floodplain L_R, the aggradation of the channel A_C, and the aggradation of the floodplain A_F (**Figure 1**). In order to measure these variables, we collected the following data from the scaled cross-sections (examples in **Figure 2**):

- A line trace of the seafloor (upper black line in **Figures 1**, **2**);
- A line trace of the base of the channel belt (lower black line in **Figures 1**, **2**);
- 2 points marking the external levee crests (red dots in **Figures 1**, **2**);
- 2 points marking the floodplain elevation (blue dots in **Figures 1**, **2**);
- 1 point marking the initial/deepest location of the channel-base (green dot in **Figures 1**, **2**).

Where available, we utilized previous authors' interpretation of the lines and points (e.g., Pirmez and Flood, 1995). Our methods for defining (1) the locations of the levee crest, channel thalweg, floodplain, and channel-belt base elevations; and (2) the derivation of channel belt metrics (e.g., H, A_C, A_F, H_{CB}) are described here and graphically depicted in **Figure 1**. The levee crest and channel thalweg are straightforward to define by using the highest and lowest point, respectively, on a cross-sectional profile of the seafloor (**Figure 1**; Shumaker et al., 2018). The channel-belt base can be defined as the deepest/lowest location that the channel occupied, which in most cases is the initial channel location at the beginning of channel-belt deposition. The channel-belt base is typically straightforward to locate in simple aggradational channel belts by using the geometries and cross-cutting relationships of the channel-belt deposits (**Figure 2**). Where the channel-belt base location was uncertain, we selected the deepest/lowest point of the interpreted channel belt (**Figures 1**, **2**). The most subjective and interpretive

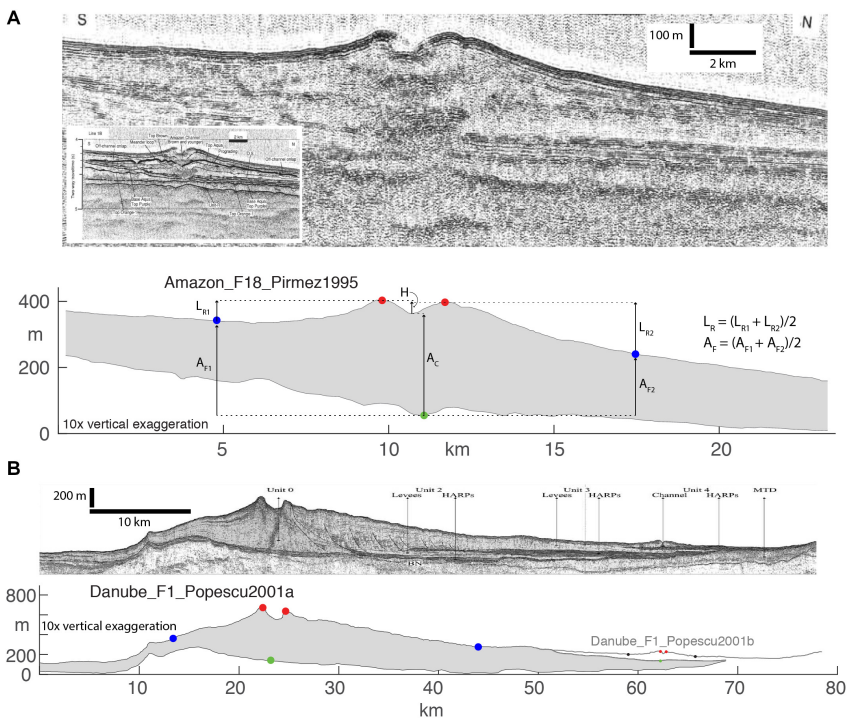

FIGURE 2 | Seismic-reflection profiles and associated measurements of the Amazon channel **(A)** and Danube channel **(B)**. Both profiles displayed at 10x vertical exaggeration but are not scaled to each other. Note the significant aggradation of the channel above the floodplain in both channels. Note also the difference in superelevation between the Danube abandoned channel (left) and the modern channel (right). Image in **(A)** from Pirmez and Flood (1995); image in **(B)** from Popescu et al. (2001).

data to collect is the floodplain elevation (i.e., the base of the levee). The location of this point can be difficult to define, given that levee relief decreases asymptotically toward the floodplain in rivers (Pizzuto, 1987; Ferguson and Brierley, 1999) and submarine channels (Normark et al., 1993; Skene et al., 2002; Straub and Mohrig, 2008; Nakajima and Kneller, 2012). We tested various methods to define the floodplain elevation, including (1) picking where the levee-slope derivative stabilizes, (2) where the levee-slope becomes asymptotic with respect to a horizontal line, and (3) fitting of power law and/or exponential equations to the levee slope. However, these methods can generate spurious results due to variations in data quality, cross-section orientation, and local factors that affect the levee such as sediment waves, gullies, faults, and older/younger channel belts on the levee (Nakajima and Kneller, 2012; **Figure 2**). Hence, we select the floodplain elevation qualitatively (i.e., via 'ocular inspection'), constraining this location according to two criteria: (1) where the levee slope becomes asymptotic to the regional floodplain – this point defines the base of the levee; and (2) where the channel-belt thickness stabilizes wth increasing distance from the channel – this defines the point where floodplain aggradation is the chief process rather than levee deposition (**Figures 1**, **2**). Generally, these two criteria are spatially correlated, but we recognize this qualitative method has inherent uncertainty. For example, selecting the floodplain elevation (i.e., base of the levee) in **Figure 2B** is more subjective than in **Figure 2A** because of data quality and complexity of antecedent topography. However, it does not appear to be possible to define the floodplain elevation in a more rigorous, quantitative manner (see discussion in Normark et al., 1993).

With the afore-mentioned points selected on a particular cross-section, two values of L_R are calculated (as shown in **Figure 1**) as the vertical distance between each levee crest points and the floodplain elevation; those two values are averaged into the final value of L_R. Two values of A_F are also calculated as the vertical distance between the floodplain elevation and the line defining the channel-belt base (**Figure 1**); again, those two values are averaged into the final value of A_F. We average the two values of L_R and A_F rather than take a maximum or minimum value because of local variations in levee morphology and variations in data quality (**Figure 2**). For example, the cross-section in **Figure 2A** is not exactly perpendicular to the flow direction of the channel, causing a slight elevation difference between the two floodplains, and an average of the two measurements alleviates this issue. The channel aggradation A_C is calculated as the vertical distance between the point marking the initial location of the channel and the channel thalweg (defined as the minimum y value of the line trace of the seafloor between the levee crests; **Figure 1**). Examples of typical seismic-reflection profiles are shown in **Figure 2**.

RESULTS

Fifty-two submarine channel-belt cross-sections are shown in **Figure 3**, with channel-base, levee crests, and floodplain elevations indicated by green, red, and blue dots, respectively. These data are derived from the modern and Quaternary channels of the following submarine fans: Amazon (n = 35; key reference is Manson, 2009), Zaire (n = 9; Picot et al., 2016), Danube (n = 3; Popescu et al., 2001), Rhone (n = 3; Bonnel et al., 2005), Magdalena (n = 1; Leslie et al., 2011), and Mississippi (n = 1; Stelting et al., 1986). Channel dimensions are consistent with other data compilations from submarine settings (**Table 1**; Konsoer et al., 2013; Shumaker et al., 2018), providing confidence in our data collection methodology.

As a proxy for sediment volume encompassed in the channel belt, we calculated the area of each channel-belt cross-section (**Figure 4**). These values are normalized by channel cross-sectional area, and the P_{10}-P_{50}-P_{90} distribution of channel-belt area is 11-84-249 channel areas. This suggests that a typical submarine channel-belt (gray area in **Figure 3A**) contains 80–100 times more sediment than the cross-sectional area of the channel (**Figure 4**). Values of fluvial channel belt area (or volume) are not available for comparison, but the channel belt data from Jobe et al. (2016) suggests that while rivers are much less aggradational, they build much wider channel belts than submarine channels; thus, both environments may have similar channel belt area values.

To enable comparison between channel-belt parameters, we compiled available data from the literature. Jobe et al. (2016) provide values of normalized channel belt thickness (H_{cb}/H) from submarine and fluvial settings, and Mohrig et al. (2000) provide values of superelevation (S_E) for rivers (**Figure 5**). Submarine channel-belts are ∼10 times thicker than fluvial channel-belts (**Figure 5**), supporting the theory developed above as well as qualitative (e.g., Peakall et al., 2000; Kolla et al., 2007) and quantitative (Jobe et al., 2016) observations. Values of submarine H_{cb}/H collected in this study are very similar to compiled data from Jobe et al. (2016; **Figure 5**); however, our H_{cb}/H values are slightly larger, likely because we focused solely on leveed, aggradational submarine channel belts, whereas Jobe et al. (2016) collected data from both erosional and constructional submarine channel belts.

The magnitude of levee relief L_R for submarine channel-belts (P_{50} of 64 m) is 10 to 70 times larger than fluvial channel-belt L_R (P_{50} of 1 m from Mohrig et al., 2000). Some larger rivers can have taller levees; for example, the Mississippi river has 6 m high levees (Shen et al., 2015) and the Rhine-Meuse river has 3–5 m high levees (Törnqvist, 1994). However, we cannot find an example of a fluvial levee > 10 m high, so an average submarine levee is still an order of magnitude taller than an average fluvial levee. This comparison is not normalized, and it is well-documented that submarine channels are larger than rivers (Konsoer et al., 2013). Normalizing levee relief by channel depth (Eq. 1; Mohrig et al., 2000) produces superelevation (S_E), which is shown in **Figure 5**. We find that submarine channel S_E values have a $P_{10-50-90}$ distribution of 0.8/1.9/4.5, while fluvial S_E values are consistently lower, with a distribution of 0.4/0.7/1.3 (**Figure 5**). From these distributions, submarine S_E values are 1.2 to 3.5 times larger than fluvial S_E values (**Figure 5**), suggesting that submarine channels can be stable when superelevated up to 3.5 channel depths above the floodplain, while rivers nearly always avulse before reaching 1 channel depth of superelevation.

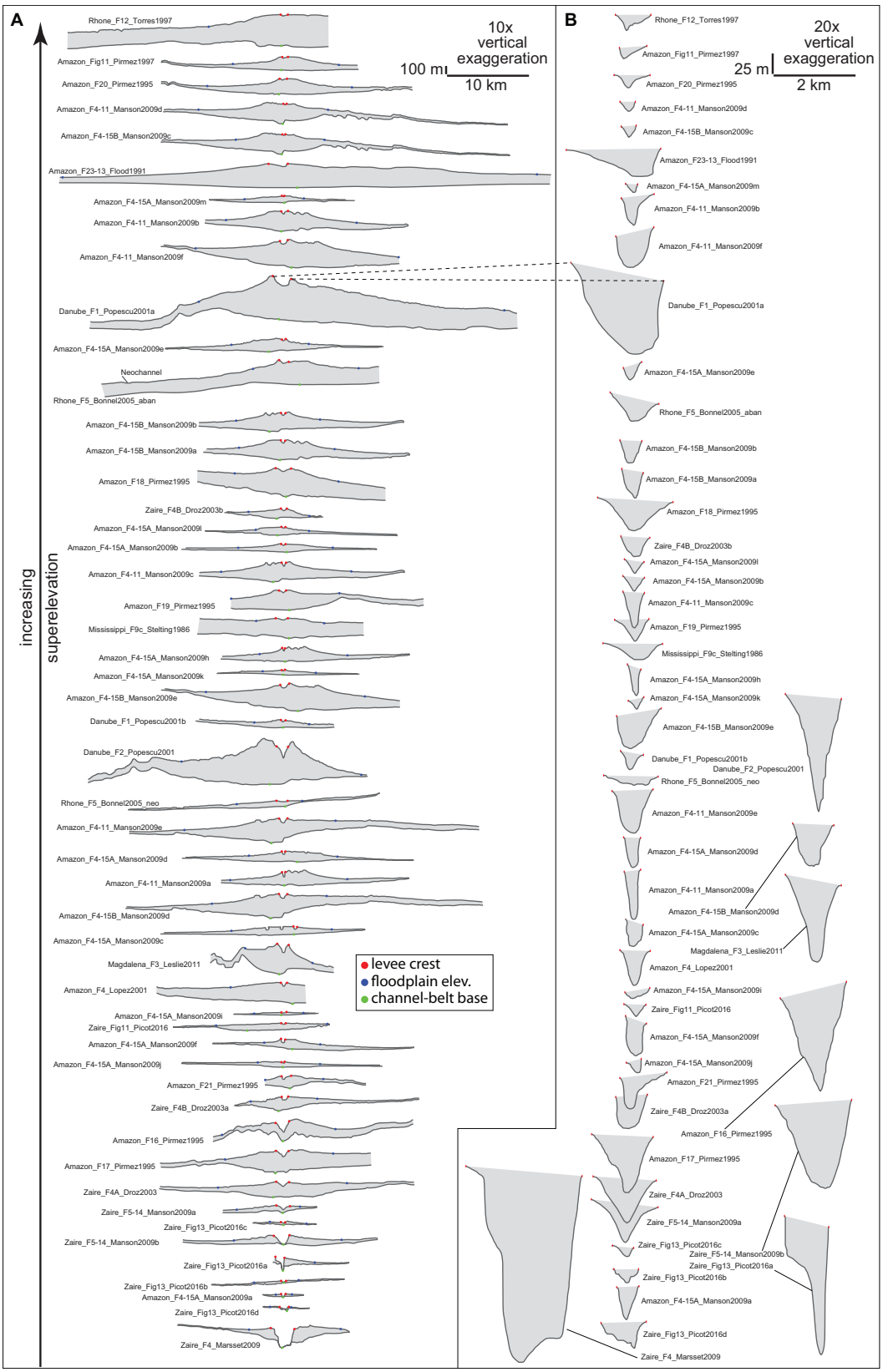

FIGURE 3 | Line tracings of 52 seismic-reflection profiles that compose this study's dataset. **(A)** Channel-belt cross-sections with red, blue, and green points showing the levee crest, floodplain elevation (i.e., base of levee), and channel-belt base, respectively. Cross-sections ordered from bottom to top in ascending superelevation value. **(B)** Zoom-in from part A of each channel, with levee crest points shown in red.

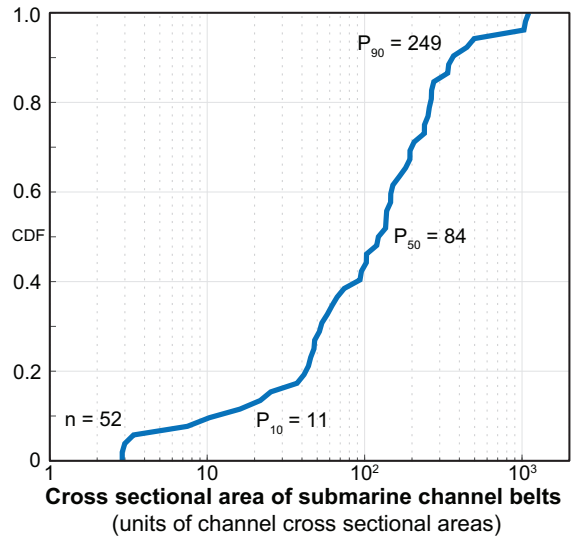

FIGURE 4 | Cross-sectional area of submarine channel belts. These data are derived from cross-sections in **Figure 3A**, and normalized by the cross-sectional area of the channel in **Figure 3B**. This data suggests that a typical submarine channel-belt contains ~ 100 times more sediment than the channel that created it.

No published values of paired A_F and A_C values from rivers were available to compute χ to compare to submarine values (**Figure 5**). However, ratios of floodplain-aggradation to channel-aggradation *rates* range from 0.02 to 0.25 for rivers (**Figure 6**; Allison et al., 1998; Makaske et al., 2002; Törnqvist and Bridge, 2002; Aalto et al., 2008). While aggradation-rate data from submarine channel-belts would be best for comparison, no reliable data exist. Hence, we simply compare the submarine A_F/A_C ratio (from thickness data) to the fluvial A_F/A_C ratio (from rate data), with the assumption that the larger values should most closely align with avulsion conditions (**Figure 6**). The submarine P_{90} and fluvial P_{10} values of A_F/A_C do not overlap (**Figure 6**), supporting the avulsion criteria discussed above, specifically: (1) A_F in fluvial channel-belts is insignificant compared to A_C and thus can be ignored when considering avulsion criteria for rivers (see Eq. 3; **Figure 1**); and (2) A_F cannot be ignored in submarine channel belts and thus must be included in the avulsion criteria (see Eq. 4; **Figure 1**). We caution that while these A_F/A_C results are intuitive and consistent with theory and available data, they should be considered preliminary until A_F/A_C rate data can be collected from submarine channel belts.

DISCUSSION

Why Are Submarine Channel Belts So Thick and Superelevated?

The results of this study clearly demonstrate that submarine channels commonly attain S_E and $\chi > 1$ (**Figure 5**), values much higher than observed in rivers. We interpret that the unique turbidity current flow properties in submarine channels are responsible for the significant superelevation and aggradation of submarine channel-belts. Flows in submarine channels have ~50 times lower density contrast between the flow and ambient fluid than rivers (Imran et al., 1998). This promotes higher sediment concentration in the upper portion of the flow, leading to levee and floodplain aggradation caused by enhanced overspill and flow stripping, particularly around channel bends (Piper and Normark, 1983; Hiscott et al., 1997). In addition, turbidity currents are strongly vertically stratified and the velocity maximum is located much closer to the bed than in a riverine flow (Sequeiros et al., 2010; Dorrell et al., 2014; Azpiroz-Zabala et al., 2017). This vertical stratification limits the potential for avulsion because: (1) the dense, energetic, coarse-grained portion of the flow remains near the channel thalweg rather than near the levee crest (Hansen et al., 2015; Jobe et al., 2017), and (2) the top of the flow has very low sediment concentration and density contrast with the ambient fluid (Imran et al., 1998) and thus little to no driving force for erosion as compared to rivers (Konsoer et al., 2013), suggesting there is diminished ability for turbidity currents to erode the external levee and trigger an avulsion. Collectively, these factors cause flows in submarine channels to have lower potential energy as compared to rivers (Imran et al., 1998; Mohrig et al., 2000). Therefore, submarine channels commonly attain larger values of levee relief, superelevation, and channel belt thickness prior to autogenic avulsion.

Submarine channel-belts also have much greater floodplain aggradation than rivers (**Figure 6**), likely because of two major sources of sediment: (1) overspill and flow-stripping from turbidity currents (Piper and Normark, 1983; Hiscott et al., 1997), which can occur at a rate of 0.3 overspill events per year (Piper and Deptuck, 1997); and (2) hemipelagic sedimentation, which can be very rapid (10–40 cm/ky) in high sediment-supply regimes where leveed submarine channels are common (Mikkelsen et al., 1997; Stow et al., 2001). The combination of muddy turbidity currents and hemipelagic deposition produces facies with rhythmically alternating very thin silt turbidite beds and bioturbated hemipelagic clay, which has been documented from many modern (e.g., Amazon channel Site 930, Hiscott et al., 1997; Normark and Damuth, 1997) and ancient submarine floodplain and 'distal external-levee' settings (Kane and Hodgson, 2011; Morris et al., 2014, 2016; Hansen et al., 2015, 2017).

Criteria for Submarine Channel Avulsion

The theory and results demonstrated above allow us to develop avulsion criteria for submarine channels. Using Eq. 8, these criteria should consist of a maximum value of S_E and χ that creates a maximum H_{CB}/H. For rivers, the avulsion criteria are $S_E = 1$, $\chi = 1$, and $H_{CB}/H = 2$ (see section "Fluvial Conditions for Avulsion"). We know that since the majority of H_{CB}/H values for submarine channel-belts are greater than 2 (**Figure 5**), avulsion values of S_E and χ must be $> > 1$. Using the distribution of fluvial S_E values shown in **Figure 5**, $S_{Efluvial} = 1$ occurs at the P_{80} position of the distribution; Mohrig et al. (2000) suggest that while 1 is the practical avulsion threshold, some rivers can attain a slightly higher superelevation before avulsing. Using this reasoning, we can use the P_{80} as a proxy for what the S_E value should be at avulsion in a submarine channel-belt; again using

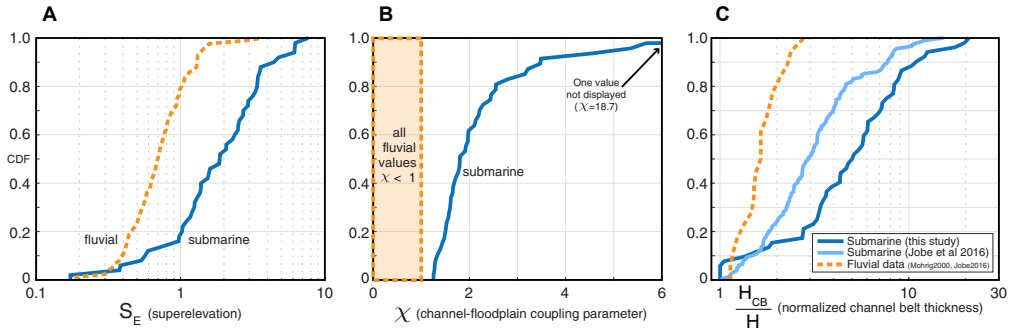

FIGURE 5 | Comparisons of fluvial and submarine channel-belt parameters superelevation **(A)**, χ coupling parameter **(B)**, and normalized channel-belt thickness **(C)**. In all cases, submarine channels show evidence for more aggradation and superelevation than rivers. These metrics suggest that avulsion criteria are very different for submarine and fluvial environments.

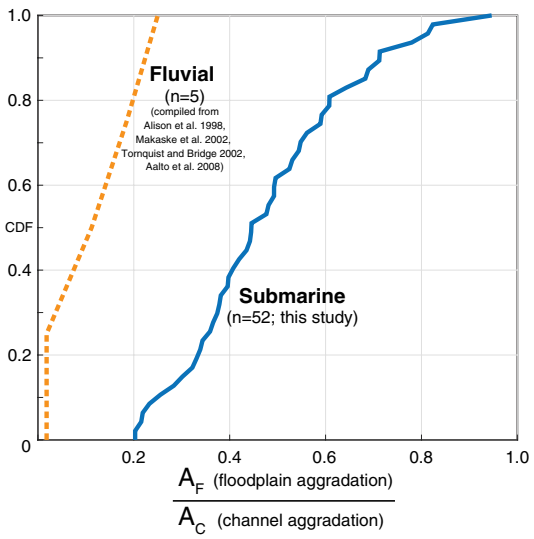

FIGURE 6 | Ratio between channel aggradation and floodplain aggradation in fluvial and submarine channel-belts. This relationship suggests that the relative contribution of floodplain aggradation is much more important in submarine channel belt growth, supporting the formulation of Eqs. 3 and 4.

Figure 5, the P_{80} $S_{E_{submarine}}$ = 3.4. Using the same reasoning for χ, the P_{80} submarine χ value is 2.5 (**Figure 5**). Revisiting Eq. 8, we can compute the value of H_{CB}/H for submarine channel-belts at avulsion:

$$S_E \sim 3.4, \quad \chi \sim 2.5, \quad \frac{H_{CB}}{H} = 1 + (S_E)(\chi),$$

$$\rightarrow \quad \frac{H_{CB}}{H} = 9.5 \; at \; avulsion$$

These avulsion thresholds are derived from our worldwide compiled dataset (n = 52), but it is important to note that these values (particularly H_{CB}/H) likely vary from system to system based on slope position, the average excess density of flows, Froude number and vertical position of the velocity maximum (Sequeiros et al., 2010), and other factors not discussed here. For example, a system with higher excess density flows may build channel belts with lower S_E and χ values, leading to an earlier avulsion (i.e., prior to attaining $H_{CB}/H \sim 9.5$). Other systems may build channels without significant levees (e.g., Picot et al., 2019) and thus promote more rapid avulsions before levee relief can develop.

To test the validity of these avulsion criteria, we construct a simple model of Eq. 8 that calculates H_{CB}/H from any value of S_E and χ (colored lines in **Figure 7A**). The independently measured H_{CB}/H values from this study (black dots and red numbers in **Figure 7A**) agree very well with the modeled H_{CB}/H values derived using Eq. 8. To quantify this agreement, **Figure 7B** cross plots the measured H_{CB}/H values (method defined in **Figures 1**, **2**) to the H_{CB}/H values calculated using Eq. 8. Although there is variability, Eq. 8 accurately predicts the observed values, with a coefficient of determination (R^2) of 0.40.

Comparison to Modern Seafloor Data

This study has focused on seismic-reflection data, where the base of the channel-belt can be confidently mapped (e.g., **Figure 2**). However, there is a wealth of publicly available bathymetry data where the concepts presented here can be observed. Three passive-margin and four active-margin channels with easily accessible bathymetry data were chosen: Amazon (Pirmez and Imran, 2003), Bengal (Schwenk et al., 2003; Kolla et al., 2012), Joshua (Posamentier, 2003), and New Zealand (Hikurangi, Bounty, Haast, and Hokitika channels; Mountjoy et al., 2009). While the Amazon and New Zealand channels have bathymetry coverage over most of their lengths, only the middle portion of the Joshua channel and the distal portion of the Bengal channel are imaged (Shumaker et al., 2018).

Figure 8A displays bathymetry-based cross-sections of the Joshua, Amazon, Bengal, and Hikurangi submarine channels, and **Figure 8B** quantifies S_E values for all seven mapped channels. Passive-margin channels (Amazon, Joshua, Bengal) show larger values of S_E and simpler seafloor topography, while active-margin channels are entrenched, with low values of S_E, and more complex seafloor topography (**Figure 8A**). The Amazon channel shows high levee relief (L_R) that decreases downstream,

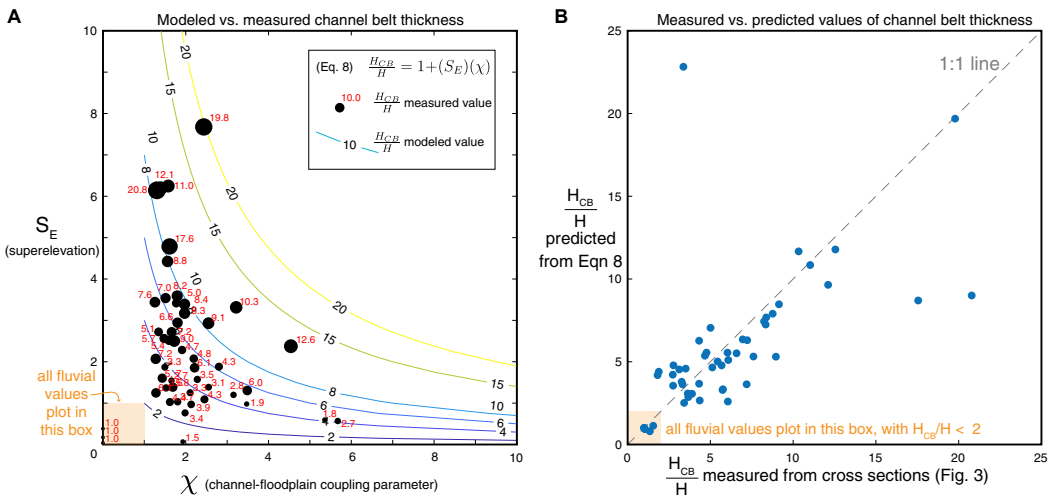

FIGURE 7 | Comparing normalized channel-belt thickness (H_{CB}/H) values measured from submarine channel cross-sections to values of H_{CB}/H modeled using Eq. 8 from this study. Note in both plots the position of fluvial values. **(A)** Plot of S_E vs. χ, with colored contour lines showing H_{CB}/H computed using Eq. 8 and the black bubbles and red text indicating the measured H_{CB}/H values. P_{80} values of S_E rarely exceeds 3.4 and P_{80} χ values rarely exceed 2.5. **(B)** Plot of measured H_{CB}/H values against computed H_{CB}/H values using Eq. 8. There is good agreement between measured and computed values of submarine H_{CB}/H. Also note that the avulsion threshold for submarine channels is approximately $H_{CB}/H = 9.5$; the majority of this study's data plots below this threshold.

consistent with previous observations (e.g., Damuth and Flood, 1983; Pirmez and Imran, 2003; Shumaker et al., 2018) and our compiled data (see next section and **Figures 9**, **10**). The Amazon and Joshua channels have very large values of S_E, up to almost 6 (**Figure 8B**), consistent with their aggradational, avulsive nature (Damuth et al., 1983; Posamentier, 2003) and slope position. Since only the distal portion and channel mouth of the studied Bengal channel has bathymetry coverage (Shumaker et al., 2018), values of S_E are small (**Figure 8B**), but more proximal data shows a more aggradational channel similar to the Joshua and Amazon (Weber et al., 1997; Schwenk and Spieß, 2009). All four of the active-margin channels near New Zealand (**Figure 8**) have high-relief submarine topography near the channel and thus are variably incised/entrenched (**Figure 8A**). Values of S_E for the four active-margin channels are $< < 1$ and do not change predictably downslope (**Figure 8**). We interpret that this difference is caused chiefly by the tectonic setting and associated seafloor deformation. While the Joshua, Amazon, and Bengal channels can build an equilibrium profile and thus have strong channel-floodplain coupling, and can aggrade a channel belt to the avulsion thresholds, the abundant seafloor topography in the Hikurangi, Haast, Bounty, and Hokitika channels creates a disequilibrium slope that perturbs the channel-floodplain coupling (**Figure 8**). Hence, these active-margin channels are less likely to reach avulsion threshold values of S_E and χ than passive-margin submarine channels.

Levee Slope as a Potential Predictor of Avulsion

There is wide variability in the lateral slope of the external levees in submarine channel belts (**Figures 3**, **8**). Intuitively, one would think that a steep levee slope would lead to more rapid avulsion. Indeed, the lateral levee slope has been proposed as an alternative (to superelevation) control on channel avulsion in rivers (Mackey and Bridge, 1995). The reasoning is that a higher levee slope leads to more rapid avulsion due to the erosional power of water on that slope, given a levee breach (see discussion in Mohrig et al., 2000). It is also geometrically intuitive that superelevation and levee slope are correlated, with the levee slope becoming steeper as superelevation increases (Slingerland and Smith, 1998). The cursory analysis of Mohrig et al. (2000) indicates that superelevation is a more reliable predictor of avulsion than levee slope by comparing both metrics from five modern rivers. We do not specifically measure levee slope because most of our cross-sections are not perfectly perpendicular to the channel flow direction (**Table 1**). However, with the burgeoning amount of high-quality topography and bathymetry data now available, a valuable future study could rigorously compare levee slopes to superelevation for submarine and fluvial channel-belts. Of particular interest would be to consider how the differing flow characteristics (e.g., excess density differences between riverine flow and turbidity currents) may influence erosion of shallow and steep levee slopes and thus avulsion.

Downstream Changes in Channel-Belt Dimensions in the Amazon Submarine Fan

The Amazon submarine sediment routing system is a well-characterized locale for understanding submarine fan/channel dynamics (Damuth and Kumar, 1975; Flood and Damuth, 1987; Pirmez and Flood, 1995; Pirmez and Imran, 2003; Jegou et al., 2008; Manson, 2009). Channel avulsion and its effects on fan growth have been demonstrated in the Amazon

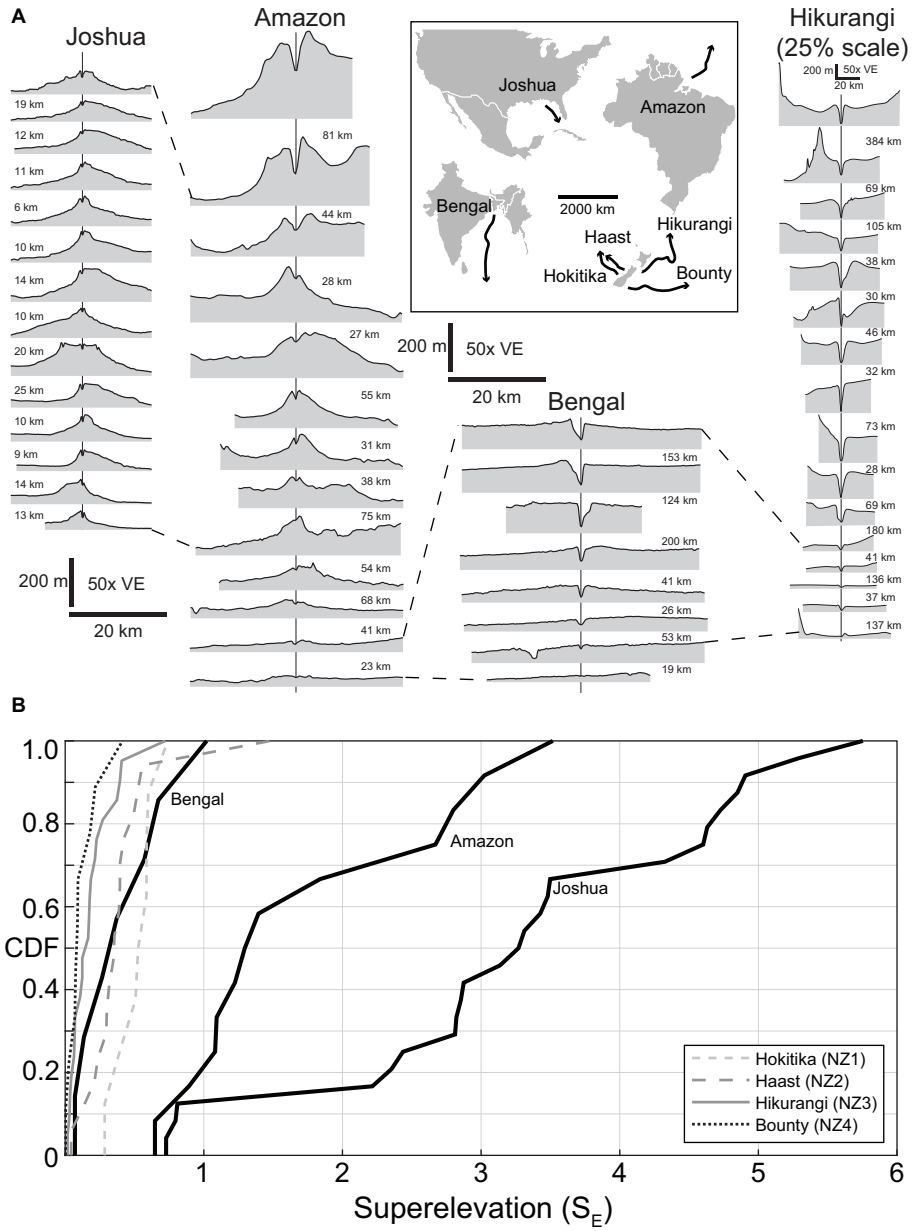

FIGURE 8 | Submarine channels on the modern seafloor show variable superelevation. **(A)** Cross-sections of modern submarine channels (inset map for location). Dashed lines indicate approximately equivalent streamwise portions of the four channels based on normalized channel length. Distance between each cross-section shown in kilometers. **(B)** Calculated superelevation values indicate that passive-margin channels commonly attain higher superelevation, perhaps due to development of an equilibrium profile and strong channel-floodplain coupling. Note that the studied portion of the Bengal channel is quite distal (see **A**), and thus not highly superelevated. The Hikurangi channel and other active-margin channels around New Zealand cannot build an equilibrium profile and thus display weak channel-floodplain coupling, with little levee development and thus low values of superelevation.

system (Damuth and Flood, 1983; Damuth et al., 1983, 1988; Flood et al., 1991; Pirmez and Flood, 1995; Piper and Normark, 2001; Manson, 2009; Maslin, 2009). Pirmez and Flood (1995) established a naming scheme for Quaternary channel avulsions on the Amazon Fan, and this study focuses on three of those named channels (**Figure 9**): 'Brown' (oldest), '1E,' and 'Amazon' (youngest, and the modern, most recently active channel). While older channels (e.g., 'Aqua,' 'Orange') and other channels/avulsions have been documented during the studied time period (e.g., 1A, 1B, 1C, 1D, 1F; see Pirmez and Flood, 1995), suitable seismic-reflection profiles are absent or insufficient for full characterization. **Figure 9** shows a map of the Brown, 1E, and Amazon channels and their associated channel-belt cross-sections. There are 16 cross-sections that intersect the Brown

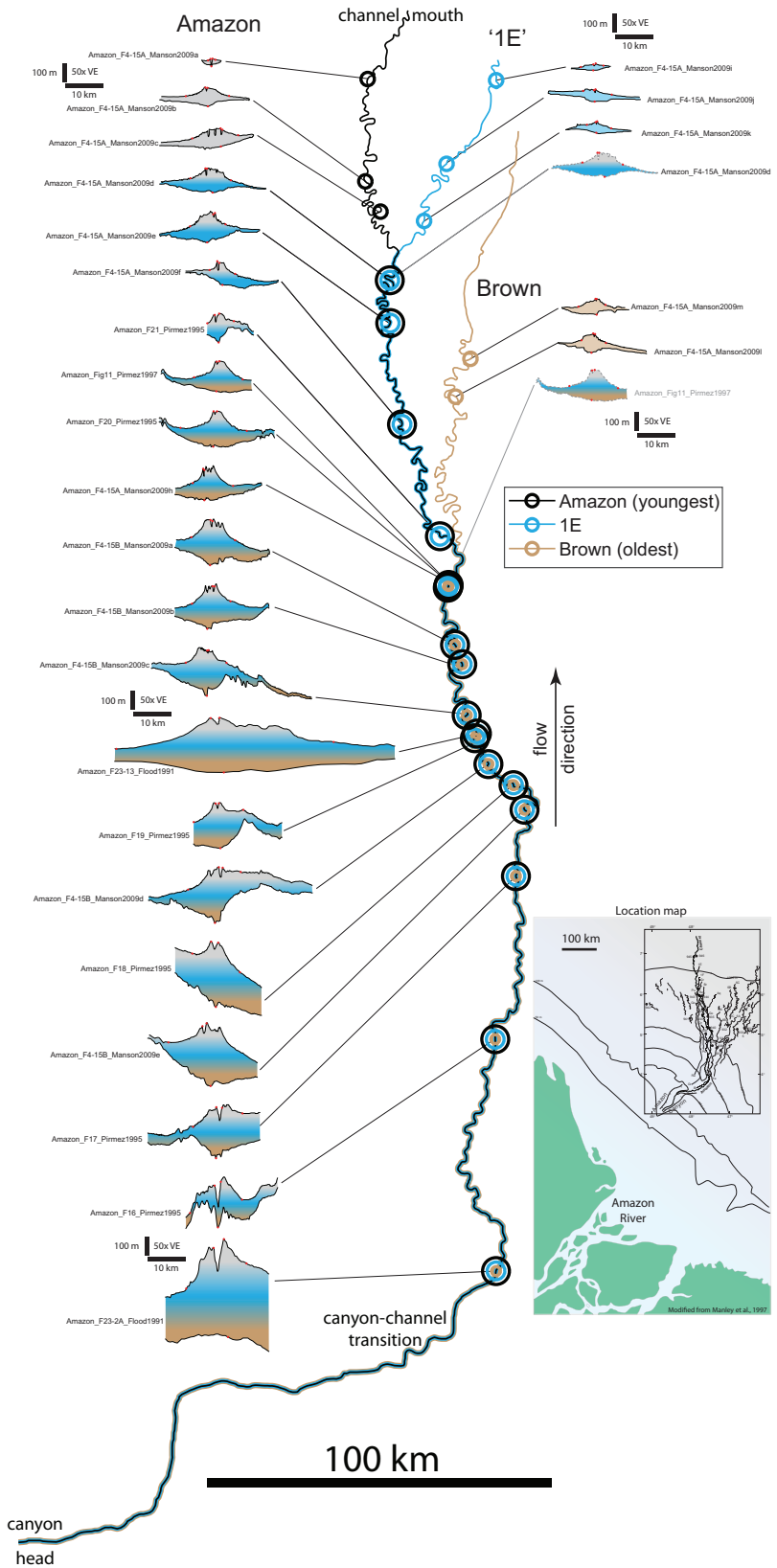

FIGURE 9 | Amazon map showing location of the Brown, 1E, and modern Amazon channel segments, as well as the location of channel cross-sections derived from seismic reflection data. Inset shows the location of the Amazon fan-channel system offshore Brazil.

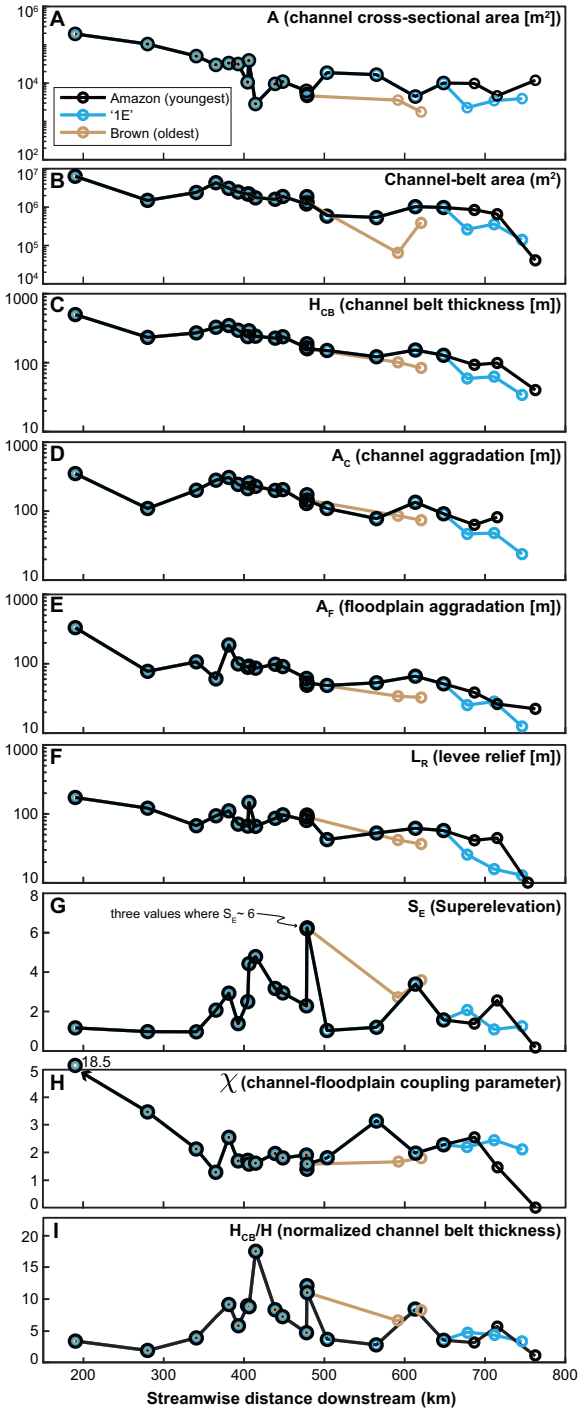

FIGURE 10 | Downstream channel-belt metrics for the Amazon submarine channel. Most channel and channel-belt metrics show a distinct downstream decrease **(A–F)**, consistent with models of channel-belt evolution and aggradation. However, superelevation **(G)** shows low values upstream (near the canyon-channel transition) and a peak near the Brown-channel avulsion node, indicating a potential linkage between superelevation and avulsion location. In **(H)**, note the consistent values of χ, indicating strong channel-floodplain coupling throughout the downstream channel evolution. Normalized channel-belt thickness **(I)** also shows this relationship, supporting the formulation of Eq. 8.

channel from the canyon-channel transition to the last mapped Brown channel location (**Figure 9**). An avulsion to the northwest created the subsequent 1E channel, which is constrained by 21 cross-sections (**Figure 9**). Finally, the most recent avulsion (again to the northwest) created the Amazon channel, which is constrained by 21 cross-sections (**Figure 9**). It is important to note that all turbidity currents that built the Brown, 1E, and Amazon channels traversed through the 14 most upstream cross-sections, denoted as vertically stacked color gradients in **Figure 9** and stacked datapoints in **Figure 10**. We measured channel-belt dimensions at each cross-section location from the seafloor to the base of the oldest channel-belt genetically linked to that cross-section (**Figure 9**; e.g., base-Brown for the 14 cross-section furthest upstream, then base-1E for the next four cross-sections, etc.). This is the most accurate method available to measure true channel-belt dimensions, but it does not account for modification of the channel and channel-belt morphology that has likely occurred post-Brown and post-1E (i.e., during development of the modern Amazon channel; **Figure 9**). Since there presently is no way to reconstruct the channel dimensions for Brown and 1E time at each cross-section location, we utilize modern seafloor channel and levee dimensions (e.g., H, L_R) to compare all three channel belts (Brown, 1E, Amazon).

Channel and channel-belt metrics generally show pronounced decreases downstream (**Figure 10**). Channel cross-sectional area in all three channel-belts (Brown, 1E, and Amazon) decreases by nearly 100x downstream (**Figure 10A**). We also computed the area of the channel belt (gray area between the points defining the floodplain, **Figure 3**) as a proxy for total sediment volume contained within the channel belt (**Figures 4**, **10B**). The channel belt area also shows a steady downstream decrease in each of the three channel belts, with nearly two orders of magnitude of total change (**Figure 10B**). Channel belt parameters that record aggradation (H_{CB}, A_F, A_C) show consistent decreasing values downstream (**Figures 10C–E**), with total change from upstream to downstream approximately 10-fold. Levee relief (L_R) also decreases consistently downstream, with upstream values near 200 m and downstream values of only 10 m (**Figure 10F**). This downstream decrease in L_R is well-documented for the Amazon channel (e.g., Figure 4 of Damuth and Flood, 1983; Piper and Normark, 2001; Pirmez and Imran, 2003) and other large, leveed submarine channels (e.g., Babonneau et al., 2002, 2010).

These downstream-thinning trends in channel-belt parameters are consistent with qualitative models of submarine fan growth (Mutti and Normark, 1987; Damuth et al., 1988). However, S_E and χ show very different trends that are related to submarine channel avulsion dynamics. Upstream S_E is relatively low ($S_E \sim 1$), but increases downstream to the Brown avulsion location, where S_E values approach 6 (**Figure 10G**). Downstream of the Brown avulsion, S_E values for Brown significantly decrease, consistent with models of autogenic channel avulsion dynamics (Brizga and Finlayson, 1990; Mohrig et al., 2000). While we cannot rule out the possibility that L_R and/or H were modified post-Brown and post-1E and these values of S_E are not accurate, the close proximity of three independently-measured cross-sections with almost identical

values of $S_E \sim 6$ (**Figures 9**, **10G**) suggests that this value may be the avulsion 'setup' for the modern Amazon channel. For the 1E channel, the avulsion location is not marked by a large S_E value (**Figure 10G**), suggesting that either (1) L_R and H are not accurately measured or have been modified by the Amazon channel at this locale, or (2) that the 1E avulsion was caused by allogenic forcing (e.g., in-channel mass transport deposition, levee failure) rather than a large value of S_E. While poor absolute age control prevents us from unequivocally demonstrating an allogenic trigger at 1E time, Maslin (2009) reports emplacement of a large mass transport deposit at approximately 1E time, supporting one potential allogenic mechanism. If these trends in downstream S_E are correct, the next autogenic avulsion in the Amazon channel should occur near the Brown channel avulsion, as this remains the highest measured S_E (**Figures 9**, **10G**). Why the channel has remained stable at this location with $S_E \sim 6$ is not clear, but this behavior suggests that submarine channels are quite stable in highly aggradational settings (cf. Dorrell et al., 2015). Channel-floodplain coupling is consistent in the Amazon, with values of $\chi \sim 2$ for approximately 400 km (**Figure 10H**). Interestingly, the Brown and 1E avulsions do not result in a change in χ, suggesting that strong channel-floodplain coupling may be inherent to submarine channels (**Figure 7A**). Modification of χ from a value of ~ 2 seems to be related to local factors; for example, very high values of χ exist in the canyon-channel transition zone, and the distalmost measurement has a very low χ value (**Figure 10H**).

Using Eq. 8, we would predict that with variable S_E and consistent χ, the normalized channel-belt thickness (H_{CB}/H) would mimic the trend of S_E. Indeed, our measurements of H_{CB}/H show the highest values just upstream of the Brown avulsion location, supporting our theory of channel-belt aggradation and avulsion. The very large H_{CB}/H measurement at $\sim$ 420 km (cross-section F23-13, Flood et al., 1991) may have been caused by the improper selection of channel-belt base, resulting in a channel belt that is falsely thick; however, this was chosen by Flood et al. (1991) and we have no data to provide an alternate interpretation.

CONCLUSION

Avulsions are important drivers for creating channelized stratigraphy in both fluvial and submarine channels, and constraining the avulsion setup is critical for predicting the distribution of sediment, organic matter, and pollutants in these sediment routing systems. The relative aggradation of the channel, external levee, and floodplain are the dominant drivers for autogenic avulsion dynamics, and they can be related in a geometric form. This study establishes a geometric channel-belt framework for predicting avulsions for both rivers and submarine channels and provides the first reported avulsion criteria for submarine channels. Prior studies have focused on superelevation of the channel above the floodplain, an important predictor of avulsion for rivers. While rivers can only superelevate an amount equivalent to 1 channel depth above the floodplain prior to avulsion, submarine channels are more stable during aggradation, and we document new data demonstrating superelevation values > 3 channel depths.

These observations result in a normalized channel-belt thickness for submarine channels that can be as thick as $\sim$ 10 channel depths, while fluvial channel belts are limited to a belt thickness of 2 channel depths. This disparity is caused by the differences in superelevation, but also by differences in channel-floodplain coupling. Since floodplain aggradation values reported from fluvial channel belts are only 1–10% compared to channel aggradation, the floodplain contributes a negligible amount to channel-belt thickness and thus can be disregarded. In submarine channels, however, floodplain aggradation is significant (up to 50% the value of channel aggradation) due to levee overspill, flow stripping, and hemipelagic deposition. We summarize these observations with a coupling parameter chi (χ) that relates floodplain aggradation to channel aggradation $A_C/(A_C\text{-}A_F)$. This coupling parameter is effectively 1 for rivers but ranges from 1 to 6 for submarine channels.

Submarine channel belts can be up to 10 times thicker than their fluvial counterparts at avulsion due to enhanced superelevation and channel-floodplain coupling, and we interpret that these enhancements are related to the unique flow properties of turbidity currents. External levee aggradation and thus superelevation is promoted by overspill from flows with 50x lower density contrast with the ambient fluid as compared to riverine flows. Submarine floodplains are aggradational as well, contributing significantly to channel-belt growth. When the channel is perched far above the floodplain (i.e., significantly superelevated), there is far less potential energy in the flow as compared to a river, leading to a stable, aggradational channel. We demonstrate this stability using downstream trends in the Amazon channel, where superelevation and the channel-floodplain coupling parameter χ remain at 2 or greater for more than 400 streamwise km, resulting in a channel belt that is $\sim$ 5 channel-depths thick, more than twice the aggradation that a river is capable of.

DATA AVAILABILITY STATEMENT

All datasets generated for this study are included in the article/supplementary material.

AUTHOR CONTRIBUTIONS

ZJ wrote the manuscript and prepared the figures. NH developed concepts and performed data analysis. KS developed concepts and co-wrote the manuscript. DC performed data collection. HD performed data analysis. LS performed data analysis. LP helped develop concepts and perform data analysis. FL helped develop concepts and perform data analysis.

ACKNOWLEDGMENTS

We thank the two reviewers DH and MJ and the associate editor AO, whose careful and thoughtful reviews greatly enhanced the quality and readability of this article. We also thank Jeremiah Moody, Oriol Falivene, John Martin, Ash Harris, Morgan Sullivan, Zoltán Sylvester, and Alessandro Cantelli for topical discussions and code-sharing. ZJ acknowledges support from Chevron through the Center of Research Excellence at Colorado School of Mines (core.mines.edu).

REFERENCES

Aalto, R., Lauer, J. W., and Dietrich, W. E. (2008). Spatial and temporal dynamics of sediment accumulation and exchange along Strickland River floodplains (Papua New Guinea) over decadal-to-centennial timescales. *J. Geophys. Res. Earth Surf.* 113:F01S04. doi: 10.1029/2006JF000627

Allison, M. A., Kuehl, S. A., Martin, T. C., and Hassan, A. (1998). Importance of flood-plain sedimentation for river sediment budgets and terrigenous input to the oceans: insights from the Brahmaputra-Jamuna River. *Geology* 26, 175–178. doi: 10.1130/0091-7613(1998)026<0175:IOFPSF>2.3.CO;2

Armitage, D. A., McHargue, T., Fildani, A., and Graham, S. A. (2012). Postavulsion channel evolution: Niger Delta continental slope. *AAPG Bull.* 96, 823–843. doi: 10.1306/09131110189

Azpiroz-Zabala, M., Cartigny, M. J. B., Talling, P. J., Parsons, D. R., Sumner, E. J., Clare, M. A., et al. (2017). Newly recognized turbidity current structure can explain prolonged flushing of submarine canyons. *Sci. Adv.* 3:e1700200. doi: 10.1126/sciadv.1700200

Babonneau, N., Savoye, B., Cremer, M., and Bez, M. (2010). Sedimentary architecture in meanders of a submarine channel: detailed study of the present Congo turbidite channel (Zaiango Project). *J. Sediment. Res.* 80, 852–866. doi: 10.2110/jsr.2010.078

Babonneau, N., Savoye, B., Cremer, M., and Klein, B. (2002). Morphology and architecture of the present canyon and channel system of the Zaire deep-sea fan. *Mar. Pet. Geol.* 19, 445–467. doi: 10.1016/S0264-8172(02)00009-0

Bonnel, C., Dennielou, B., Droz, L., Mulder, T., and Berné, S. (2005). Architecture and depositional pattern of the Rhône Neofan and recent gravity activity in the Gulf of Lions (western Mediterranean). *Mar. Pet. Geol.* 22, 827–843. doi: 10.1016/j.marpetgeo.2005.03.003

Bridge, J. S., and Leeder, M. R. (1979). A simulation model of alluvial stratigraphy. *Sedimentology* 26, 617–644. doi: 10.1111/j.1365-3091.1979.tb00935.x

Brizga, S. O., and Finlayson, B. L. (1990). Channel avulsion and river metamorphosis: the case of the Thomson River, Victoria, Australia. *Earth Surf. Process. Landf.* 15, 391–404. doi: 10.1002/esp.3290150503

Brunt, R. L., Di Celma, C. N., Hodgson, D. M., Flint, S. S., Kavanagh, J. P., and Van Der Merwe, W. C. (2013). Driving a channel through a levee when the levee is high: an outcrop example of submarine down-dip entrenchment. *Mar. Pet. Geol.* 41, 134–145. doi: 10.1016/j.marpetgeo.2012.02.016

Bryant, M., Falk, P., and Paola, C. (1995). Experimental study of avulsion frequency and rate of deposition. *Geology* 23, 365–368.

Buffington, E. C. (1952). Submarine" Natural Levees". *J. Geol.* 60, 473–479. doi: 10.1086/625999

Burns, C. E., Mountney, N. P., Hodgson, D. M., and Colombera, L. (2017). Anatomy and dimensions of fluvial crevasse-splay deposits: examples from the Cretaceous Castlegate Sandstone and Neslen Formation, Utah, U.S.A. *Sediment. Geol.* 351, 21–35. doi: 10.1016/j.sedgeo.2017.02.003

Damuth, J. E., and Flood, R. D. (1983). Morphology, sedimentation processes, and growth pattern of the Amazon deep-sea fan. *Geo Mar. Lett.* 3, 109–117. doi: 10.1007/bf02462455

Damuth, J. E., Flood, R. D., and Kowsmann, R. O. (1988). Anatomy and growth pattern of Amazon deep-sea fan as revealed by long-range side-scan sonar (GLORIA) and high-resolution seismic studies. *Am. Assoc. Petrol. Geol. Bull.* 72, 885–911.

Damuth, J. E., Kowsmann, R. O., Flood, R. D., Belderson, R. H., and Gorini, M. A. (1983). Age relationships of distributary channels on Amazon deep-sea fan: implications for fan growth pattern. *Geology* 11, 470–473.

Damuth, J. E., and Kumar, N. (1975). Amazon Cone: morphology, sediments, age, and growth pattern. *Geol. Soc. Am. Bull.* 86, 863–878.

Dietrich, W. E., and Whiting, P. (1989). "Boundary shear stress and sediment transport in river meanders of sand and gravel," in *River Meandering*, eds S. Ikeda and G. Parker (Washington, DC: American Geophysical Union), 1–50. doi: 10.1029/wm012p0001

Dorrell, R. M., Burns, A. D., and McCaffrey, W. D. (2015). The inherent instability of leveed seafloor channels. *Geophys. Res. Lett.* 42, 4023–4031. doi: 10.1002/2015gl063809

Dorrell, R. M., Darby, S. E., Peakall, J., Sumner, E. J., Parsons, D. R., and Wynn, R. B. (2014). The critical role of stratification in submarine channels: implications for channelization and long runout of flows. *J. Geophys. Res. Oceans* 119, 2620–2641. doi: 10.1002/2014jc009807

Droz, L., Marsset, T., Ondras, H., and Lopez, M. (2003). Architecture of an active mud-rich turbidite system: the Zaire Fan (Congo–Angola margin southeast Atlantic): results from ZaAngo 1 and 2 cruises. *AAPG Bull.* 87, 1145–1168. doi: 10.1306/03070300013

Edmonds, D. A., Hoyal, D. C. J. D., Sheets, B. A., and Slingerland, R. L. (2009). Predicting delta avulsions: implications for coastal wetland restoration. *Geology* 37, 759–762. doi: 10.1130/G25743A.1

Ferguson, R. J., and Brierley, G. J. (1999). Levee morphology and sedimentology along the lower Tuross River, south—eastern Australia. *Sedimentology* 46, 627–648. doi: 10.1046/j.1365-3091.1999.00235.x

Fernandes, A. M., Törnqvist, T. E., Straub, K. M., and Mohrig, D. (2016). Connecting the backwater hydraulics of coastal rivers to fluvio-deltaic sedimentology and stratigraphy. *Geology* 44, 979–982. doi: 10.1130/g37965.1

Fildani, A., Normark, W. R., Kostic, S., and Parker, G. (2006). Channel formation by flow stripping: large-scale scour features along the Monterey East Channel and their relation to sediment waves. *Sedimentology* 53, 1265–1287. doi: 10.1111/j.1365-3091.2006.00812.x

Flood, R. D., and Damuth, J. E. (1987). Quantitative characteristics of sinuous distributary channels on the Amazon deep-sea fan. *Geol. Soc. Am. Bull.* 98, 728–738.

Flood, R. D., Manley, P. L., Kowsmann, R. O., Appi, C. J., and Pirmez, C. (1991). *Seismic Facies and Late Quaternary Growth of Amazon Submarine Fan BT – Seismic Facies and Sedimentary Processes of Submarine Fans and Turbidite Systems, in Seismic Facies and Sedimentary Processes of Submarine Fans and Turbidite Systems*. New York, NY: Springer, 415–433.

Flood, R. D., Pirmez, C., and Yin, H. (1997). "The compressional-wave velocity of Amazon fan sediments: calculation from index properties and variation with clay content," in *Proceedings of the Ocean Drilling Program, Scientific Results*, College Station, TX.

Ganti, V., Chadwick, A. J., Hassenruck-Gudipati, H. J., and Lamb, M. P. (2016). Avulsion cycles and their stratigraphic signature on an experimental backwater-controlled delta. *J. Geophys. Res. Earth Surf.* 121, 1651–1675. doi: 10.1002/2016jf003915

Hajek, E. A., and Edmonds, D. A. (2014). Is river avulsion style controlled by floodplain morphodynamics? *Geology* 42, 199–202. doi: 10.1130/G35045.1

Hansen, L., Callow, R., Kane, I., and Kneller, B. (2017). Differentiating submarine channel-related thin-bedded turbidite facies: outcrop examples from the Rosario Formation, Mexico. *Sediment. Geol.* 358, 19–34. doi: 10.1016/j.sedgeo.2017.06.009

Hansen, L., Callow, R. H. T., Kane, I. A., Gamberi, F., Rovere, M., Cronin, B. T., et al. (2015). Genesis and character of thin-bedded turbidites associated with submarine channels. *Mar. Pet. Geol.* 67, 852–879. doi: 10.1016/j.marpetgeo.2015.06.007

Hay, A. E. (1987). Turbidity currents and submarine channel formation in Rupert Inlet, British Columbia: 2. The roles of continuous and surge—type flow. *J. Geophys. Res.* 92, 2883–2900.

Heller, P. L., and Paola, C. (1996). Downstream changes in alluvial architecture; an exploration of controls on channel-stacking patterns. *J. Sediment. Res.* 66, 297–306.

Hiscott, R. N., Hall, F. R., and Pirmez, C. (1997). Turbidity-current overspill from the Amazon Channel: texture of the silt/sand load, paleoflow from anisotropy of

magnetic susceptibility, and implications for flow processes. *Proc. Ocean Drill. Prog. Sci. Results* 155, 53–78.

Hodgson, D. M., Bernhardt, A., Clare, M., Silva, A., Fosdick, J., Mauz, B., et al. (2018). Grand challenges (and great opportunities) in sedimentology, stratigraphy, and diagenesis research. *Front. Earth Sci.* 6:173. doi: 10.3389/feart.2018.00173

Hübscher, C., Spieβ, V., Breitzke, M., and Weber, M. E. (1997). The youngest channel-levee system of the Bengal Fan: results from digital sediment echosounder data. *Mar. Geol.* 141, 125–145. doi: 10.1016/s0025-3227(97)00066-2

Imran, J., Parker, G., and Katopodes, N. (1998). A numerical model of channel inception on submarine fans. *J. Geophys. Res.* 103, 1219–1238. doi: 10.1029/97jc01721

Imran, J., Parker, G., and Pirmez, C. (1999). A nonlinear model of flow in meandering submarine and subaerial channels. *J. Fluid Mech.* 400, 295–331. doi: 10.1017/s0022112099006515

Jegou, I., Savoye, B., Pirmez, C., and Droz, L. (2008). Channel-mouth lobe complex of the recent Amazon Fan: the missing piece. *Mar. Geol.* 252, 62–77. doi: 10.1016/j.margeo.2008.03.004

Jerolmack, D. J. (2009). Conceptual framework for assessing the response of delta channel networks to Holocene sea level rise. *Quat. Sci. Rev.* 28, 1786–1800. doi: 10.1016/j.quascirev.2009.02.015

Jerolmack, D. J., and Paola, C. (2007). Complexity in a cellular model of river avulsion. *Geomorphology* 91, 259–270. doi: 10.1016/j.geomorph.2007.04.022

Jobe, Z. R., Howes, N. C., and Auchter, N. C. (2016). Comparing submarine and fluvial channel kinematics: implications for stratigraphic architecture. *Geology* 44, 931–934. doi: 10.1130/G38158.1

Jobe, Z. R., Lowe, D. R., and Uchytil, S. J. (2011). Two fundamentally different types of submarine canyons along the continental margin of Equatorial Guinea. *Mar. Pet. Geol.* 28, 843–860. doi: 10.1016/j.marpetgeo.2010.07.012

Jobe, Z. R., Sylvester, Z., Pittaluga, M. B., Frascati, A., Pirmez, C., Minisini, D., et al. (2017). Facies architecture of submarine channel deposits on the western Niger Delta slope: implications for grain-size and density stratification in turbidity currents. *J. Geophys. Res. Earth Surf.* 122, 473–491. doi: 10.1002/2016jf003903

Johnston, G. H., David, S. R., and Edmonds, D. A. (2019). Connecting fluvial levee deposition to flood—basin hydrology. *J. Geophys. Res. Earth Surf.* 124, 1996–2012. doi: 10.1029/2019jf005014

Jones, L. S., and Schumm, S. A. (1999). "Causes of avulsion: an overview," in *Fluvial Sedimentology VI. International Association of Sedimentologists Special Publication 28*, eds N. D. Smith and J.Rogers (Oxford: Blackwell Science), 171–178.

Kane, I. A., and Clare, M. A. (2019). Dispersion, accumulation, and the ultimate fate of microplastics in deep—marine environments: a review and future directions. *Front. Earth Sci.* 7:80. doi: 10.3389/feart.2019.00080

Kane, I. A., and Hodgson, D. M. (2011). Sedimentological criteria to differentiate submarine channel levee subenvironments: exhumed examples from the Rosario Fm. (Upper Cretaceous) of Baja California, Mexico, and the Fort Brown Fm. (Permian), Karoo Basin, S. Africa. *Mar. Pet. Geol.* 28, 807–823. doi: 10.1016/j.marpetgeo.2010.05.009

Kolla, V. (2007). A review of sinuous channel avulsion patterns in some major deep-sea fans and factors controlling them. *Mar. Pet. Geol.* 24, 450–469. doi: 10.1016/j.marpetgeo.2007.01.004

Kolla, V., Bandyopadhyay, A., Gupta, P., Mukherjee, B., and Ramana, D. V. (2012). "Morphology and internal structure of a recent upper Bengal fan valley complex," in *Application of the Principles of Seismic Geomorphology to Continental-Slope and Base-of-Slope Systems: Case Studies from Seafloor and Near-seafloor Analogues*, eds B. E. Prather, M.E. Deptuck, D. Mohrig, B. Van Horn, and R.B. Wynn (Broken Arrow, OK: Society for Sedimentary Geology), 347–369. doi: 10.2110/pec.12.99.0347

Kolla, V., Posamentier, H. W., and Wood, L. J. (2007). Deep-water and fluvial sinuous channels—characteristics, similarities and dissimilarities, and modes of formation. *Mar. Pet. Geol.* 24, 388–405. doi: 10.1016/j.marpetgeo.2007.01.007

Konsoer, K., Zinger, J., and Parker, G. (2013). Bankfull hydraulic geometry of submarine channels created by turbidity currents: relations between bankfull channel characteristics and formative flow discharge. *J. Geophys. Res. Earth Surf.* 118, 216–228. doi: 10.1029/2012JF002422

Leeder, M. R. (1978). "A quantitative stratigraphic model for alluvium, with special reference to channel deposit density and interconnectedness," in *Fluvial Sedimentology, Canadian Society of Petroleum. Geologists Memoirs 5*, ed. A. Miall (Hoboken, NJ: John Wiley & Sons, Inc.), 587–596.

Leslie, S., Cordon, I., and Lopez-Gamundi, O. (2011). *Pleistocene to Recent Channel / Levee System From the Slope of the Magdalena Fan*. Available online at: http://www.earthdoc.org/publication/publicationdetails/?publication=66227

Lewin, J., and Ashworth, P. J. (2014). The negative relief of large river floodplains. *Earth Sci. Rev.* 129, 1–23. doi: 10.1016/j.earscirev.2013.10.014

Lopez, M. (2001). Architecture and depositional pattern of the Quaternary deep-sea fan of the Amazon. *Mar. Pet. Geol.* 18, 479–486. doi: 10.1016/s0264-8172(00)00071-4

Mackey, S. D., and Bridge, J. S. (1995). Three-dimensional model of alluvial stratigraphy; theory and applications. *J. Sediment. Res.* 65, 7–31. doi: 10.1306/d42681d5-2b26-11d7-8648000102c1865d

Makaske, B., Smith, D. G., and Berendsen, H. J. A. (2002). Avulsions, channel evolution and floodplain sedimentation rates of the anastomosing upper Columbia River, British Columbia, Canada. *Sedimentology* 49, 1049–1071. doi: 10.1046/j.1365-3091.2002.00489.x

Manson, S. (2009). *Avulsion Process : Stratigraphic and Lithologic Records – Application to the Amazon and Zaire Turbidite Systems*. Brest: Université de Bretagne occidentale – Brest.

Marsset, T., Droz, L., Dennielou, B., and Pichon, E. (2009). "Cycles in the architecture of the Quaternary Zaire turbidite system: a possible link with climate," *External Controls on Deep-Water Depositional Systems. SEPM Special Publication 92*, eds B. Kneller, O. J. Martinsen, and B. McCaffrey (Tulsa, OK: SEPM Special Publication), 89–106. doi: 10.2110/sepmsp.092.089

Martin, J., Fernandes, A. M., Pickering, J., Howes, N., Mann, S., and McNeil, K. (2018). The stratigraphically preserved signature of persistent backwater dynamics in a large paleodelta system: the mungaroo formation, North West Shelf, Australia. *J. Sediment. Res.* 88, 850–872. doi: 10.2110/jsr.2018.38

Maslin, M. A. (2009). "Review of the timing and causes of the Amazon-Fan mass transport and avulsion deposits during the latest Pleistocene," *External Controls on Deep-Water Depositional Systems*, Vol. 92, eds B. Kneller, O. J. Martinsen, and B. McCaffrey (Tulsa, OK: SEPM Special Publication), 133–144. doi: 10.2110/sepmsp.092.133

Mikkelsen, N., Maslin, M., Giraudeau, J., and Showers, W. (1997). "Biostratigraphy and sedimentation rates of the Amazon Fan," in *Proceedings of the Ocean Drilling Program, Scientific Results, 155*, eds R. D. Flood, D. J. W. Piper, A. Klaus, and L. C. Peterson (College Station, TX: Ocean Drilling Program), 577–594.

Mohrig, D., Heller, P. L., and Paola, C. (2000). Interpreting avulsion process from ancient alluvial sequences: Guadalope-Matarranya system (northern Spain) and Wasatch Formation (western Colorado). *Geol. Soc. Am. Bull.* 112, 1787–1803.

Morris, E. A., Hodgson, D. M., Brunt, R. L., and Flint, S. S. (2014). Origin, evolution and anatomy of silt-prone submarine external levées. *Sedimentology* 61, 1734–1763. doi: 10.1111/sed.12114

Morris, E. A., Hodgson, D. M., Flint, S. S., and Brunt, R. L. (2016). Integrating outcrop and subsurface data to assess the temporal evolution of a submarine channel-levee system. *AAPG Bull.* 100, 1663-1691.

Mountjoy, J. J., Barnes, P. M., and Pettinga, J. R. (2009). Morphostructure and evolution of submarine canyons across an active margin: cook strait sector of the Hikurangi Margin, New Zealand. *Mar. Geol.* 260, 45–68. doi: 10.1016/j.margeo.2009.01.006

Mutti, E., and Normark, W. R. (1987). "Comparing examples of modern and ancient turbidite systems: problems and concepts," in *Marine Clastic Sedimentology*, eds J. K. Leggett and G. G. Zuffa (Dordrecht: Springer), 1–38. doi: 10.1007/978-94-009-3241-8_1

Nakajima, T., and Kneller, B. C. (2012). Quantitative analysis of the geometry of submarine external levées. *Sedimentology* 60, 877–910. doi: 10.1111/j.1365-3091.2012.01366.x

Nienhuis, J. H., Törnqvist, T. E., and Esposito, C. R. (2018). Crevasse splays versus avulsions: a recipe for land building with levee breaches. *Geophys. Res. Lett.* 45, 4058–4067. doi: 10.1029/2018GL077933

Nittrouer, J. A., Mohrig, D., Allison, M. A., and Peyret, A.-P. B. (2011). The lowermost Mississippi River: a mixed bedrock-alluvial channel. *Sedimentology* 58, 1914–1934. doi: 10.1111/j.1365-3091.2011.01245.x

Nittrouer, J. A., Shaw, J., Lamb, M. P., and Mohrig, D. (2012). Spatial and temporal trends for water-flow velocity and bed-material sediment transport in the lower Mississippi River. *Geol. Soc. Am. Bull.* 124, 400–414. doi: 10.1130/b30497.1

Normark, W. R., and Damuth, J. E. (1997). "Sedimentary facies and associated depositional elements of the Amazon Fan," in *Proceedings of the Ocean Drilling Program, Scientific Results, 155*. (College Station, TX: Ocean Drilling Program).

Normark, W. R., Posamentier, H., and Mutti, E. (1993). Turbidite systems: state of the art and future directions. *Rev. Geophys.* 31, 91–116. doi: 10.1029/93RG02832

Ortiz-Karpf, A., Hodgson, D. M., and McCaffrey, W. D. (2015). The role of mass-transport complexes in controlling channel avulsion and the subsequent sediment dispersal patterns on an active margin: the Magdalena Fan, offshore Colombia. *Mar. Pet. Geol.* 64, 58–75. doi: 10.1016/j.marpetgeo.2015.01.005

Peakall, J., McCaffrey, B., and Kneller, B. (2000). A process model for the evolution, morphology, and architecture of sinuous submarine channels. *J. Sediment. Res.* 70, 434–448. doi: 10.1306/2dc4091c-0e47-11d7-8643000102c1865d

Picot, M., Droz, L., Marsset, T., Dennielou, B., and Bez, M. (2016). Controls on turbidite sedimentation: insights from a quantitative approach of submarine channel and lobe architecture (Late Quaternary Congo Fan). *Mar. Pet. Geol.* 72, 423–446. doi: 10.1016/j.marpetgeo.2016.02.004

Picot, M., Marsset, T., Droz, L., Dennielou, B., Baudin, F., and Hermoso, M. (2019). Monsoon control on channel avulsions in the late Quaternary Congo Fan. *Quat. Sci. Rev.* 204, 149–171. doi: 10.1016/j.quascirev.2018.11.033

Piper, D. J. W., and Deptuck, M. (1997). "Fine-grained turbidites of the Amazon Fan: facies characterization and interpretation," in *Proceedings of the Ocean Drilling Program, Scientific Results, 155* (College Station, TX: Ocean Drilling Program).

Piper, D. J. W., and Normark, W. R. (1983). Turbidite depositional patterns and flow characteristics, Navy submarine fan, California borderland. *Sedimentology* 30, 681–694. doi: 10.1111/j.1365-3091.1983.tb00702.x

Piper, D. J. W., and Normark, W. R. (2001). Sandy fans–from Amazon to Hueneme and beyond. *AAPG Bull.* 85, 1407–1438.

Pirmez, C., and Flood, R. D. (1995). "Morphology and structure of Amazon channel," in *Proceedings of the Ocean Drilling Program, Initial Reports, 155* (College Station, TX: Ocean Drilling Program).

Pirmez, C., Hiscott, R. N., and Kronen, J. (1997). "Sandy turbidite successions at the base of channel-levee systems on the Amazon Fan: unraveling the facies architecture of large submarine fans," in *Proceedings of the Ocean Drilling Program, Scientific Results, 155* (College Station, TX: Ocean Drilling Program).

Pirmez, C., and Imran, J. (2003). Reconstruction of turbidity currents in Amazon Channel. *Mar. Pet. Geol.* 20, 823–849. doi: 10.1016/j.marpetgeo.2003.03.005

Pizzuto, J. E. (1987). Sediment diffusion during overbank flows. *Sedimentology* 34, 301–317. doi: 10.1111/j.1365-3091.1987.tb00779.x

Popescu, I., Lericolais, G., Panin, N., Wong, H. K., and Droz, L. (2001). Late Quaternary channel avulsions on the Danube deep-sea fan. *Black Sea Mar. Geol.* 179, 25–37. doi: 10.1016/s0025-3227(01)00197-9

Posamentier, H. W. (2003). Depositional elements associated with a basin floor channel-levee system: case study from the Gulf of Mexico. *Mar. Pet. Geol.* 20, 677–690. doi: 10.1016/j.marpetgeo.2003.01.002

Schwenk, T., Spiess, V., Hübscher, C., and Breitzke, M. (2003). Frequent channel avulsions within the active channel–levee system of the middle Bengal Fan—an exceptional channel–levee development derived from Parasound and Hydrosweep data. *Deep Sea Res. Part II Top. Stud. Oceanogr.* 50, 1023–1045. doi: 10.1016/s0967-0645(02)00618-5

Schwenk, T., and Spieß, V. (2009). "Architecture and stratigraphy of the Bengal Fan as response to tectonic and climate revealed from high-resolution seismic data," in *External Controls on Deep-Water Depositional Systems*, Vol. 92, eds B. C. Kneller, O. J. Martinsen, and B. McCaffrey (Tulsa, OK: SEPM Special Publication), 107–131. doi: 10.2110/sepmsp.092.107

Sequeiros, O. E., Spinewine, B., and Beaubouef, R. T. (2010). Characteristics of velocity and excess density profiles of saline underflows and turbidity currents flowing over a mobile bed. *J. Hydraul. Eng.* 136, 412–433. doi: 10.1061/(asce)hy.1943-7900.0000200

Shen, Z., Törnqvist, T. E., Mauz, B., Chamberlain, E. L., Nijhuis, A. G., and Sandoval, L. (2015). Episodic overbank deposition as a dominant mechanism of floodplain and delta-plain aggradation. *Geology* 43, 875–878. doi: 10.1130/G36847.1

Shumaker, L. E., Jobe, Z. R., and Graham, S. A. (2017). Evolution of submarine gullies on a prograding slope: insights from 3D seismic reflection data. *Mar. Geol.* 393, 35–46. doi: 10.1016/j.margeo.2016.06.006

Shumaker, L. E., Jobe, Z. R., Johnstone, S. A., Pettinga, L. A., Cai, D., and Moody, J. D. (2018). Controls on submarine channel-modifying processes identified through morphometric scaling relationships. *Geosphere* 14, 1–17. doi: 10.1130/GES01674.1

Skene, K. I, Piper, D. J. W., and Hill, P. S. (2002). Quantitative analysis of variations in depositional sequence thickness from submarine channel levees. *Sedimentology* 49, 1411–1430. doi: 10.1046/j.1365-3091.2002.00506.x/full

Slingerland, R., and Smith, N. D. (1998). Necessary conditions for a meandering-river avulsion. *Geology* 26, 435–438.

Slingerland, R., and Smith, N. D. (2004). River avulsions and their deposits. *Annu. Rev. Earth Planet. Sci.* 32, 257–285. doi: 10.1146/annurev.earth.32.101802.120201

Smith, N. D., Cross, T. A., Dufficy, J. P., and And Clough, S. R. (1989). Anatomy of an avulsion. *Sedimentology* 36, 1–23. doi: 10.1111/j.1365-3091.1989.tb00817.x

Stelting, C. E., Droz, L. I., Bouma, A. H., Coleman, J. M., Cremer, M., Meyer, A. W., et al. (1986). "Late pleistocene seismic stratigraphy of the Mississippi Fan," in *Initial Reports of the Deep Sea Drilling Project*, Vol. 96, eds A. H. Bouma, J. M. Coleman, and J. M. Brooks (Washington, DC: U.S. Government Printing Office), 437–456.

Stow, D. A. V., Huc, A. Y., and Bertrand, P. (2001). Depositional processes of black shales in deep water. *Mar. Pet. Geol.* 18, 491–498. doi: 10.1016/s0264-8172(01)00012-5

Stow, D. A. V., and Piper, D. J. W. (1984). Deep-water fine-grained sediments: facies models. *Geol. Soc. Lond. Spec. Publ.* 15, 611–646. doi: 10.1144/gsl.sp.1984.015.01.38

Straub, K. M., and Mohrig, D. (2008). Quantifying the morphology and growth of levees in aggrading submarine channels. *J. Geophys. Res.* 113:F03012. doi: 10.1029/2007JF000896

Straub, K. M., Mohrig, D., McElroy, B., Buttles, J., and Pirmez, C. (2008). Interactions between turbidity currents and topography in aggrading sinuous submarine channels: a laboratory study. *Geol. Soc. Am. Bull.* 120, 368–385. doi: 10.1130/B25983.1

Strong, N., and Paola, C. (2008). Valleys that never were: time surfaces versus stratigraphic surfaces. *J. Sediment. Res.* 78, 579–593. doi: 10.2110/jsr.2008.059

Sylvester, Z., Pirmez, C., and Cantelli, A. (2011). A model of submarine channel-levee evolution based on channel trajectories: implications for stratigraphic architecture. *Mar. Pet. Geol.* 28, 716–727. doi: 10.1016/j.marpetgeo.2010.05.012

Törnqvist, T. E., and Bridge, J. S. (2002). Spatial variation of overbank aggradation rate and its influence on avulsion frequency. *Sedimentology* 49, 891–905. doi: 10.1046/j.1365-3091.2002.00478.x

Torres, J., Droz, L., Savoye, B., Terentieva, E., Cochonat, P., Kenyon, N. H., et al. (1997). Deep−sea avulsion and morphosedimentary evolution of the Rhône Fan Valley and Neofan during the Late Quaternary (north−western Mediterranean Sea). *Sedimentology* 44, 457–477. doi: 10.1046/j.1365-3091.1997.d01-36.x

Törnqvist, T. E. (1994). Middle and late Holocene avulsion history of the River Rhine (Rhine-Meuse delta, Netherlands). *Geology* 22, 711–714. doi: 10.1130/0091-76131994022<0711:MALHAH<2.3.CO;2

van Toorenenburg, K. A., Donselaar, M. E., and Weltje, G. J. (2018). The life cycle of crevasse splays as a key mechanism in the aggradation of alluvial ridges and river avulsion. *Earth Surf. Process. Landf.* 43, 2409–2420. doi: 10.1002/esp.4404

Weber, M. E., Wiedicke, M. H., Kudrass, H. R., Hübscher, C., and Erlenkeuser, H. (1997). Active growth of the Bengal Fan during sea-level rise and highstand. *Geology* 25, 315–318. doi: 10.1130/0091-76131997025<0315:AGOTBF<2.3.CO

Wolman, M. G., and Leopold, L. B. (1957). River flood plains: some observations on their formation. *U.S. Geol. Surv. Prof. Pap.* 282-C, 87–109. doi: 10.1002/etc.411

Conflict of Interest: NH was employed by company Mathworks.

The remaining authors declare that the research was conducted in the absence of any commercial or financial relationships that could be construed as a potential conflict of interest.